Influence of triphosphine ligand coordination geometry in Mn(I) hydride complexes [(P∩P∩P)(CO)$_2$MnH] on their kinetic hydricity

Sergey A. Kovalenko,[a]† Ekaterina S. Gulyaeva,[a,b]† Elena S. Osipova,[a]† Oleg A. Filippov,*[a] Anastasia A. Danshina,[a] Laure Vendier,[b] Nikolay V. Kireev,[a] Ivan A. Godovikov,[a] Yves Canac,*[b] Dmitry A. Valyaev,*[b] Natalia V. Belkova[a] and Elena S. Shubina*[a]

a - A. N. Nesmeyanov Institute of Organoelement Compounds (INEOS), Russian Academy of Sciences, 28/1 Vavilov str., GSP-1, B-334, Moscow, 119334, Russia

E-mails: h-bond@ineos.ac.ru, shu@ineos.ac.ru

b - LCC-CNRS, Université de Toulouse, CNRS, 205 route de Narbonne 31077 Toulouse, Cedex 4, France. E-mail: yves.canac@lcc-toulouse.fr, dmitry.valyaev@lcc-toulouse.fr

Electronic Supplementary Information

Table of contents

Table S1. Crystallographic data and refinement parameters for Mn(I) complexes. S2

Table S2. Calculated thermodynamic and IR data for complexes [(**L1**)Mn(CO)$_2$H] and [(**L1**)Mn(CO)$_2$]$^+$ S3

Table S3. Calculated thermodynamic and IR data for complexes [(**L1-L2**)Mn(CO)$_2$(Solv)]$^+$ S3

Figure S1-S25. NMR spectra of isolated Mn(I) complexes and reaction intermediates S4

Figure S26. Variable temperature IR spectra of the *mer*-**1^H** and 1.5 equiv. B(C$_6$F$_5$)$_3$ mixture S29

Figure S27. IR spectra of *mer*-**1^H** and its mixture with 1.5 equiv. of B(C$_6$F$_5$)$_3$ at 160 K, 170 K, 190 K S29

Figure S28. IR spectra of equimolar mixture *fac*-**2^H** and B(C$_6$F$_5$)$_3$ at 260 K and after CO bubbling S30

Kinetic study of the hydrogen abstraction from complexes *mer*-**1^H** and *fac*-**2^H** to Lewis acid.....S31

Table S4. Experimentally determined current concentrations of the components in the reaction between *mer*-**1^H** and B(C$_6$F$_5$)$_3$ in *n*BuCl at 170 K.....S31

Figure S29. Plot for the determination of effective rate constant (k_{eff}) of the reaction between *mer*-**1^H** with B(C$_6$F$_5$)$_3$ in *n*BuCl at 170 K.....S31

Table S5. Calculated effective rate constants (k_{eff}) from the experimental data obtained for the reaction of *mer*-**1^H** with of B(C$_6$F$_5$)$_3$ at 170 - 200 K.....S31

Figure S30. IR monitoring of the reaction of complex *mer*-**1^H** with B(C$_6$F$_5$)$_3$ in 160-200 K temperature range and the Eyring plot of effective rate constants *vs.* 1/T S32

Table S6. Calculated effective rate constants (k_{eff}) from the experimental data obtained for the reaction of *fac*-**2^H** with of B(C$_6$F$_5$)$_3$ at 190 - 230 K.....S32

Figure S31. IR monitoring of the reaction of complex *fac*-**2^H** with B(C$_6$F$_5$)$_3$ in 190-230 K temperature range and the Eyring plot of effective rate constants *vs.* 1/T S33

Figure S32. ^{1}H NMR spectrum of crude product obtained from the hydrosilylation of benzyl benzoate catalyzed by complex *mer*-**1^{Br}** S33

Figure S33. ^{1}H NMR spectrum of crude product obtained from the hydrosilylation of benzyl benzoate catalyzed by complex *fac*-**2^{Br}** S34

Figure S34. IR spectrum of the aliquot of the reaction mixture of *fac*-**2^{Br}**,benzyl benzoate and PhSiH$_3$ S34

Table S1. Crystallographic data and refinement parameters for Mn(I) complexes.

Complex	*mer*-**1**^{Br}	*mer*-**1**^{H}	*mer*-[**1**^{MeCN}](BF_4)	*fac*-**2**^{Br}	*fac*-[**2**^{MeCN}](BF_4)
Empirical formula	$C_{36}H_{33}BrMnO_2P_3$	$C_{36}H_{34}MnO_2P_3$	$C_{38}H_{36}BF_4MnNO_2P_3$	$C_{43}H_{39}BrMnO_2P_3$	$C_{46}H_{44}BCl_2F_4MnNO_2P_3$
Fw	725.38	646.48	773.34	815.50	948.38
T, K	100	120	100	180	100
λ/Å	1.54184	0.71073	0.71073	1.54184	0.71073
Crystal system	Monoclinic	Monoclinic	Triclinic	Orthorhombic	Triclinic
Space group	$P2_1/c$	$P2_1/n$	P-1	$Pna2_1$	P-1
Z	4	4	2	4	2
a, Å	11.17670(10)	8.5939(3)	10.0848(2)	18.2707(3)	9.1917(8)
b, Å	14.61930(10)	30.4974(11)	12.3770(3)	11.9106(2)	14.0017(14)
c, Å	19.90860(10)	12.3138(5)	14.8709(3)	16.9843(4)	17.7856(16)
α, °	90	90	75.6390(10)	90	80.196(6)
β, °	97.4430(10)	100.7900(10)	84.2430(10)	90	76.870(6)
γ, °	90	90	85.3860(10)	90	80.423(4)
V, $Å^3$	3225.57(4)	3170.3(2)	1786.13(7)	3696.04(12)	2177.1(4)
D_{calc} (g cm^{-1})	1.494	1.354	1.438	1.466	1.447
m, cm^{-1}	6.437	5.99	5.61	5.686	5.93
F(000)	1480	1344	796	1672	976
θ_{max}/°	71.8	30.0	30.0	71.4	27.0
Completeness to θ_{max} (%)	0.992	0.999	0.997	0.998	0.954
Reflections measured	47377	38962	36759	34397	16953
Independent reflections	6264	8433	9461	6920	9048
Observed reflections [I > 2σ(I)]	5992	5493	6649	6173	5564
Parameters	388	379	452	534	557
R1	0.0222	0.0458	0.0472	0.035	0.1107
wR2	0.0555	0.0983	0.1167	0.0767	0.2774
GOF	1.029	1.029	1.028	1.041	1.113
$\Delta\rho_{max}$/ $\Delta\rho_{min}$ (e $Å^{-3}$)	0.308/−0.412	0.389/−0.570	0.511/−0.420	0.225/−0.251	1.785/−0.648

Table S2. Thermodynamic and IR data for different isomers of [(**L1**)Mn(CO)$_2$H] (**1^H**) and [(**L1**)Mn(CO)$_2$]$^+$ (**1$^+$**) obtained by DFT calculations.[a]

configuration	*fac*-(*sP*)-**1^H**	*fac*-(*cP*)-**1^H**	*mer,syn-(CO)*-**1^H**	*mer,anti-(CO)*-**1^H**	*mer*-(*cP*)-**1^H**
ΔE, kcal·mol^{-1}	0.1	5.6	2.0	0.0	5.2
ΔH^{298}, kcal·mol^{-1}	0.0	5.7	1.8	0.0	4.7
ΔG^{298}, kcal·mol^{-1}	1.6	8.3	2.5	0.0	4.6
ν(CO)$_1$, cm^{-1}	1995	2003	1975	1996	1981
A(CO)$_1$, km·mol^{-1}	1245	1120	1323	1158	1922
ν(CO)$_2$, cm^{-1}	2048	2054	2038	2050	2048
A(CO)$_2$, km·mol^{-1}	1286	1433	1121	1039	257
	fac-(*sP*)-**1$^+$**	*fac*-(c*P*)-**1$^+$**	*mer,syn-(CO)*-**1$^+$**	*mer,anti-(CO)*-**1$^+$**	*mer*-(*cP*)-**1$^+$**
ΔE, kcal·mol^{-1}	-6.8	-0.6	-7.6	0.0	5.6
ΔH^{298}, kcal·mol^{-1}	-5.7	0.2	-7.4	0.0	5.9
ΔG^{298}, kcal·mol^{-1}	-3.7	3.0	-5.8	0.0	6.9
ν(CO)$_1$, cm^{-1}	2050	2057	2036	2049	2047
A(CO)$_1$, km·mol^{-1}	1226	1085	944	913	1834
ν(CO)$_2$, cm^{-1}	2101	2106	2099	2100	2138
A(CO)$_2$, km·mol^{-1}	1116	1277	1049	957	174

[a] Calculation were carried out with ωB97XD functional and def2-TZVP basis set in toluene (SMD model). Relative energies are referenced to the *mer,anti-(CO)*-isomers, ν_{CO} frequencies are reported unscaled.

Table S3. Calculated thermodynamic and IR data for cationic complexes [(**L1**)Mn(CO)$_2$(Solv)]$^+$ and [(**L2**)Mn(CO)$_2$(Solv)]$^+$ (Solv = none, CH_2Cl_2, MeCN).[a]

	fac-(*sP*)-[**1^{Solv}**]$^+$			*mer,anti-(CO)*-[**1^{Solv}**]$^+$			*mer,syn-(CO)*-[**1^{Solv}**]$^+$			*fac*-[**2^{Solv}**]$^+$		
	cat	DCM	MeCN	cat	DCM	MeCN	cat	DCM	MeCN	cat	DCM	MeCN
ν(CO)$_1$, cm^{-1}	2050	2042	2044	2049	2046	2042	2036	ol	2034	2050	2042	2040
ν(CO)$_2$, cm^{-1}	2101	2096	2093	2100	2093	2088	2099		2093	2101	2098	2091
Δν(cat-MeCN)		-8			-11			-6			-10	
Δν(cat-DCM)		-5			-7			-6			-3	
Δν(DCM-MeCN)		2			4			0			7	
ΔEf, kcal·mol^{-1}		-6.0	-25.3		-8.6	-28.1		-3.3	-23.6		-4.5	-25.5
ΔHf, kcal·mol^{-1}		-5.3	-24.0		-6.4	-26.2		-1.4	-21.6		-2.8	-23.3
ΔGf, kcal·mol^{-1}		6.8	-11.5		6.9	-14.2		10.0	-9.5		10.5	-9.7

[a] Calculation were carried out with ωB97XD functional and def2-TZVP basis set in toluene (SMD model), ν_{CO} frequencies are reported unscaled.

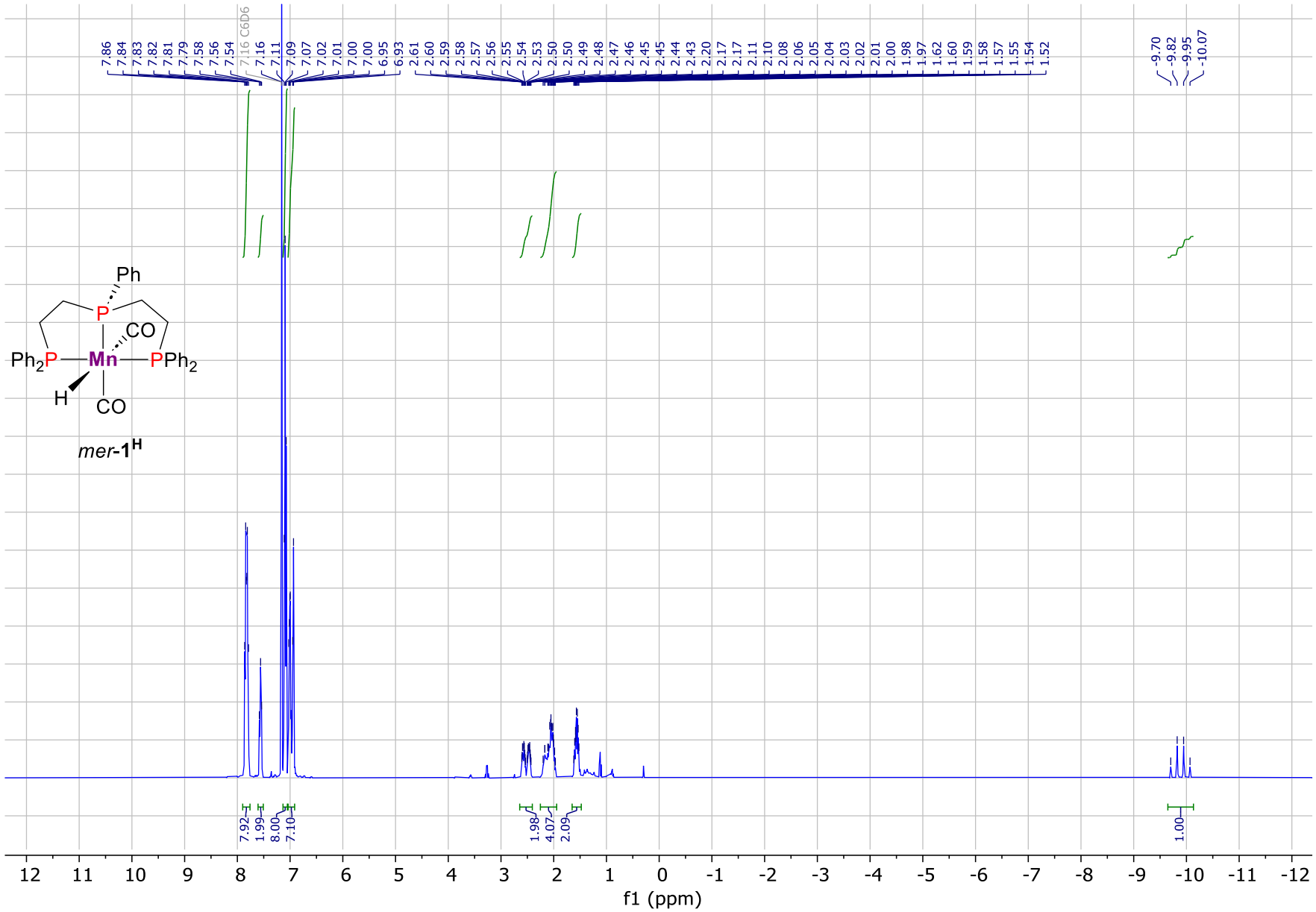

Figure S1. ^{1}H NMR spectrum of complex *mer*-**1^{H}** (400.1 MHz, C_6D_6, 298 K).

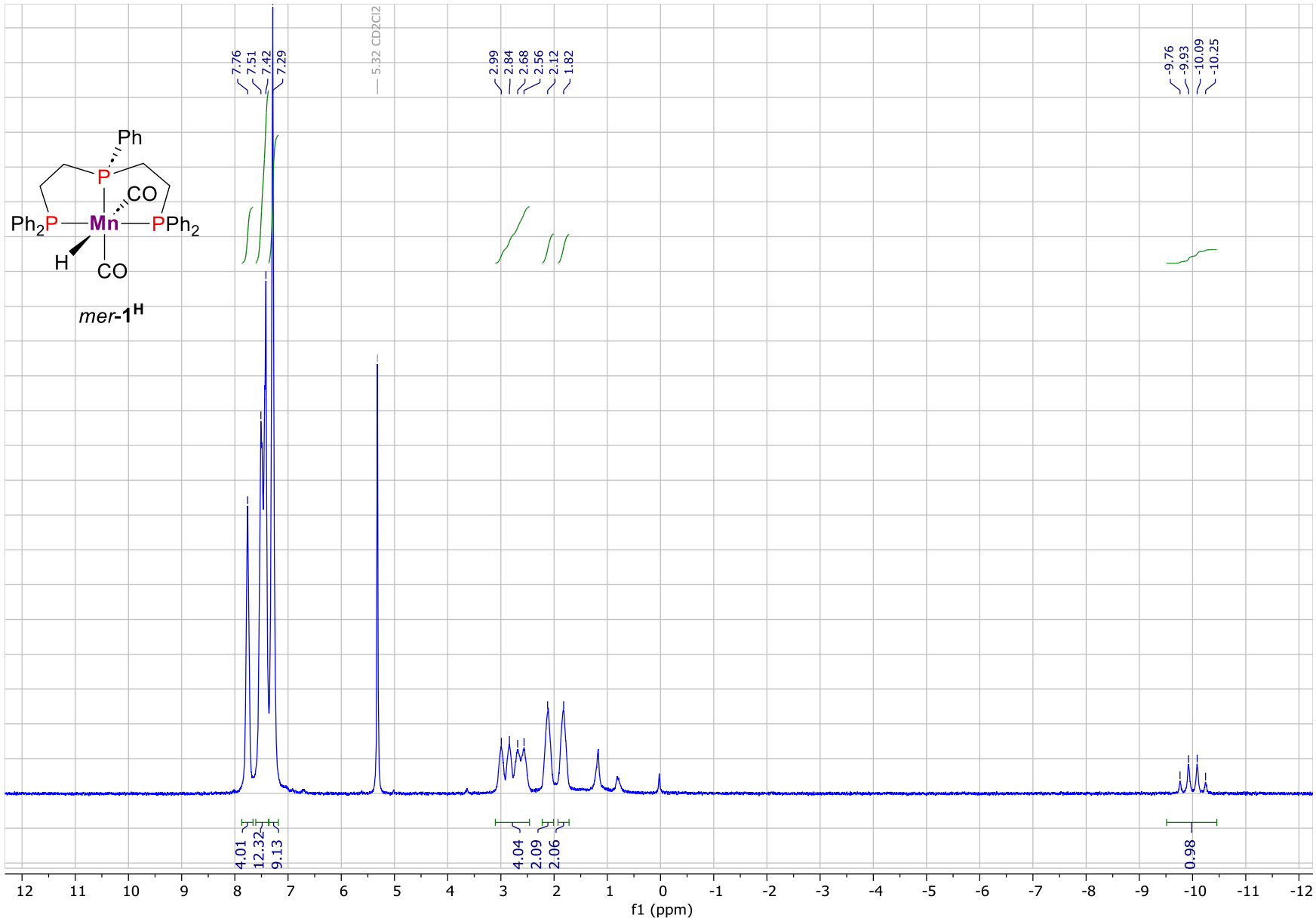

Figure S2. ^{1}H NMR spectrum of complex *mer*-**1^{H}** (300.1 MHz, CD_2Cl_2, 200 K).

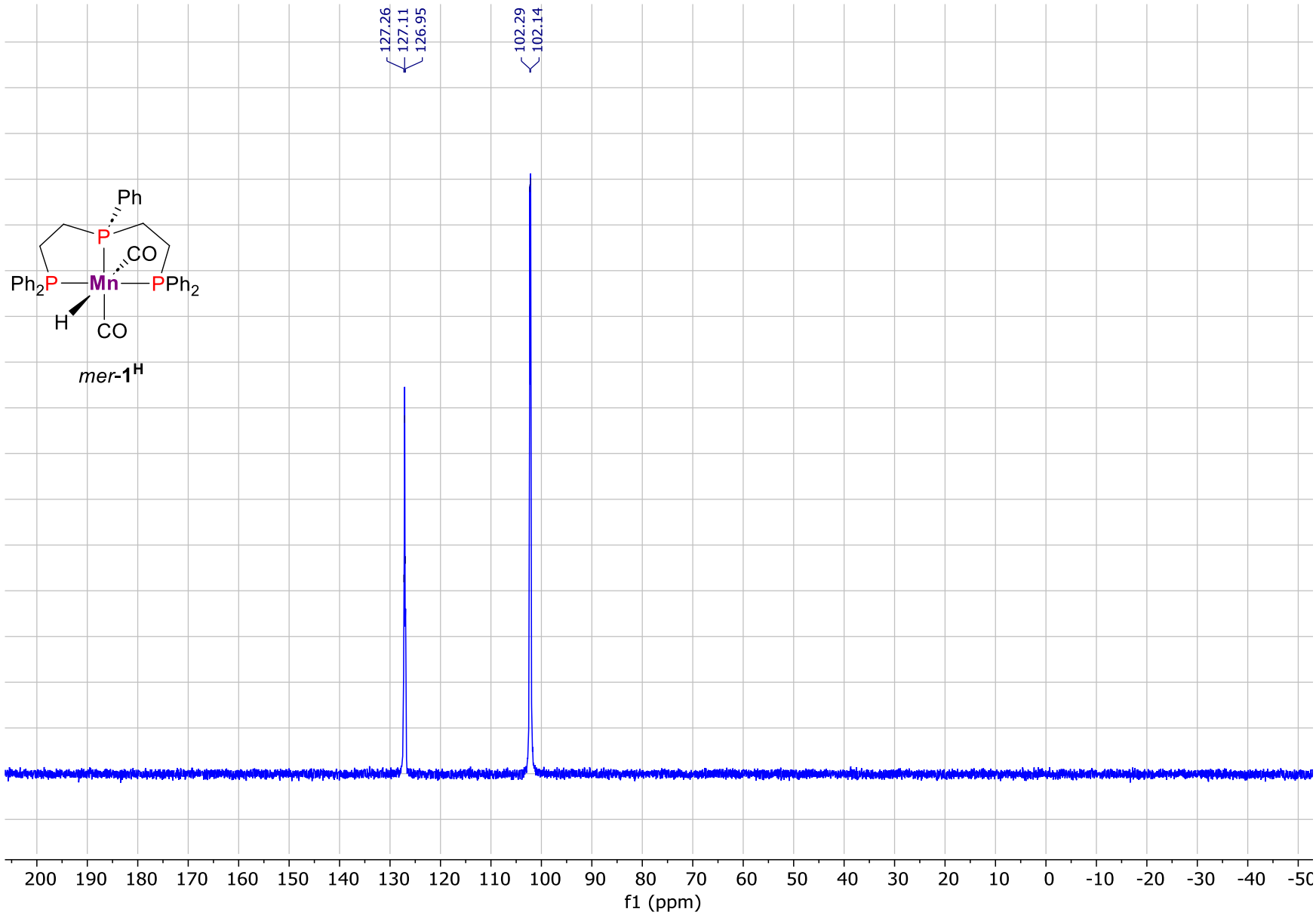

Figure S3. $^{31}P\{^{1}H\}$ NMR spectrum of complex *mer*-**1**^{H} (162.0 MHz, C_6D_6, 298 K).

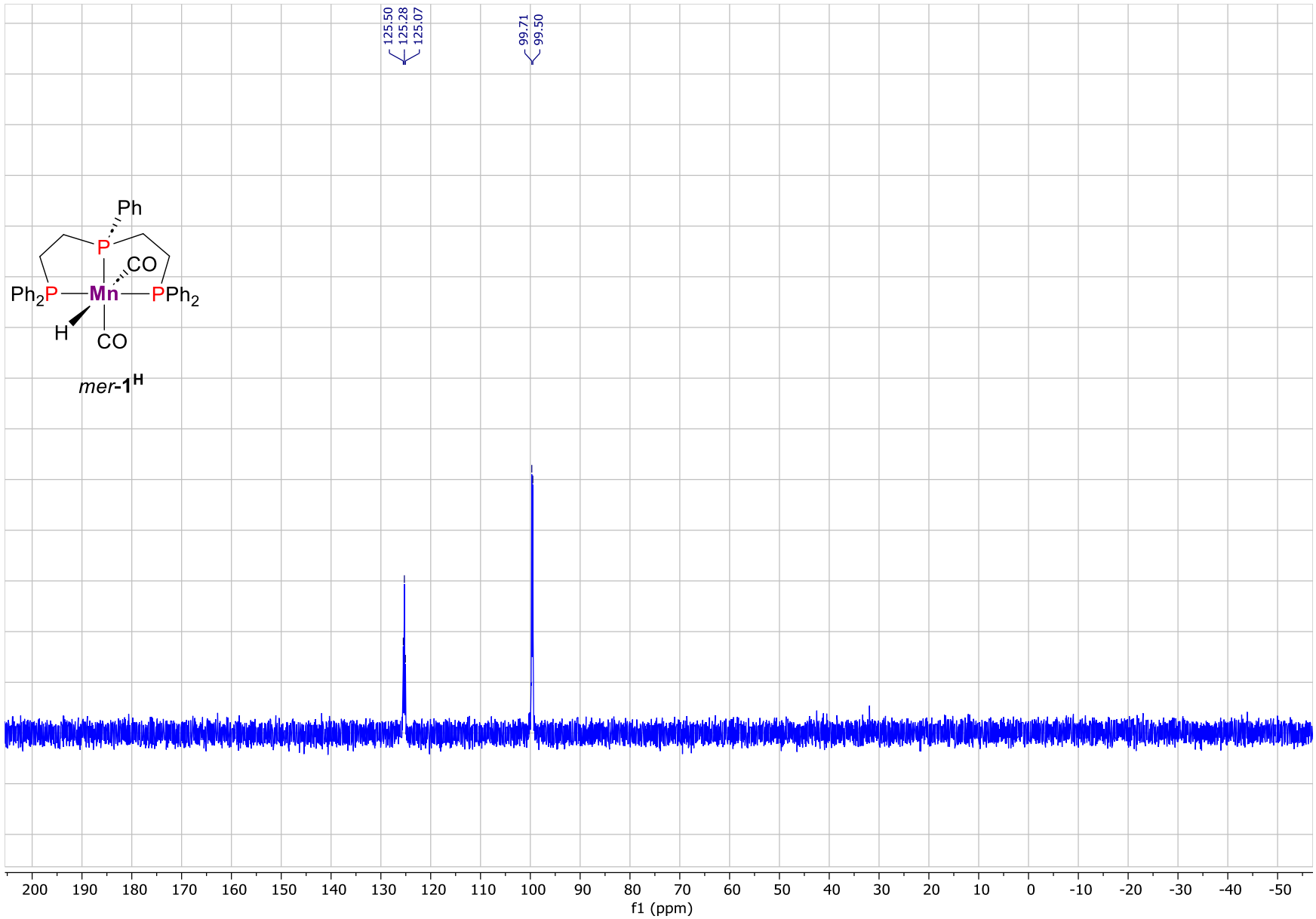

Figure S4. $^{31}P\{^{1}H\}$ NMR spectrum of complex *mer*-**1**^{H} (162.0 MHz, CD_2Cl_2, 200 K).

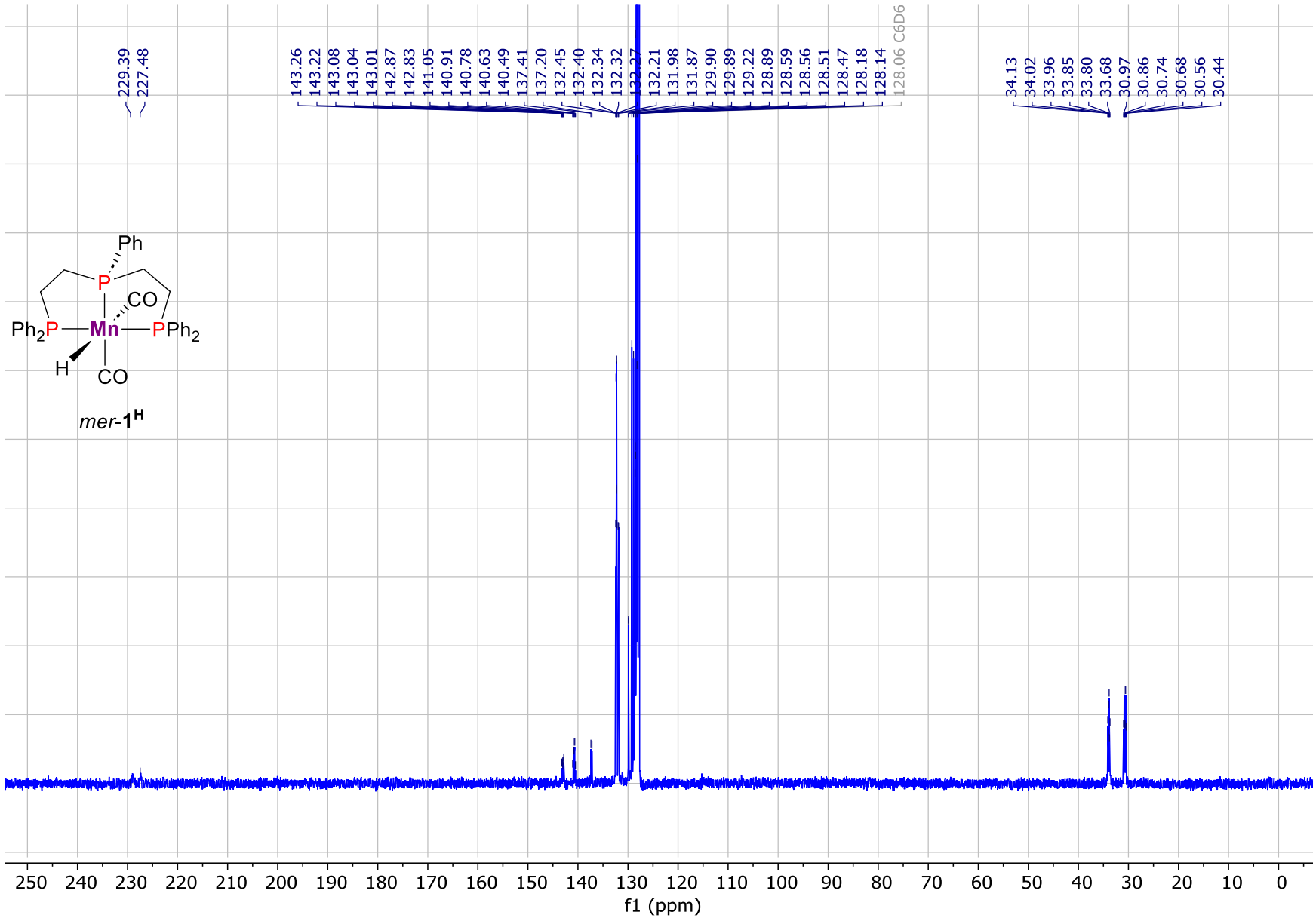

Figure S5. $^{13}C\{^{1}H\}$ NMR spectrum of complex *mer*-**1**^{H} (100.6 MHz, C_6D_6, 298 K).

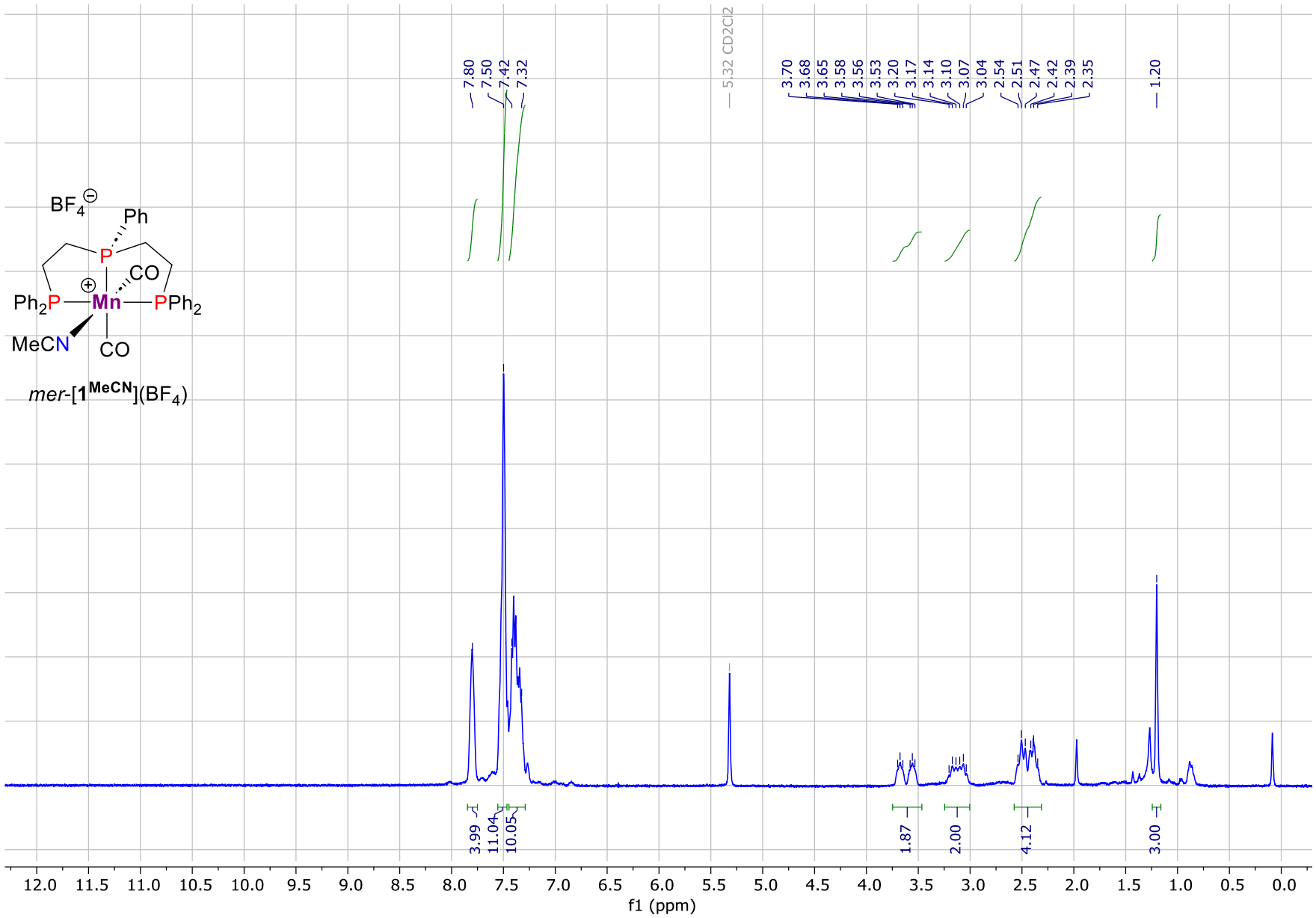

Figure S6. ^{1}H NMR spectrum of complex *mer*-[**1**$^{\mathbf{MeCN}}$](BF$_4$) (400.1 MHz, CD_2Cl_2, 298 K).

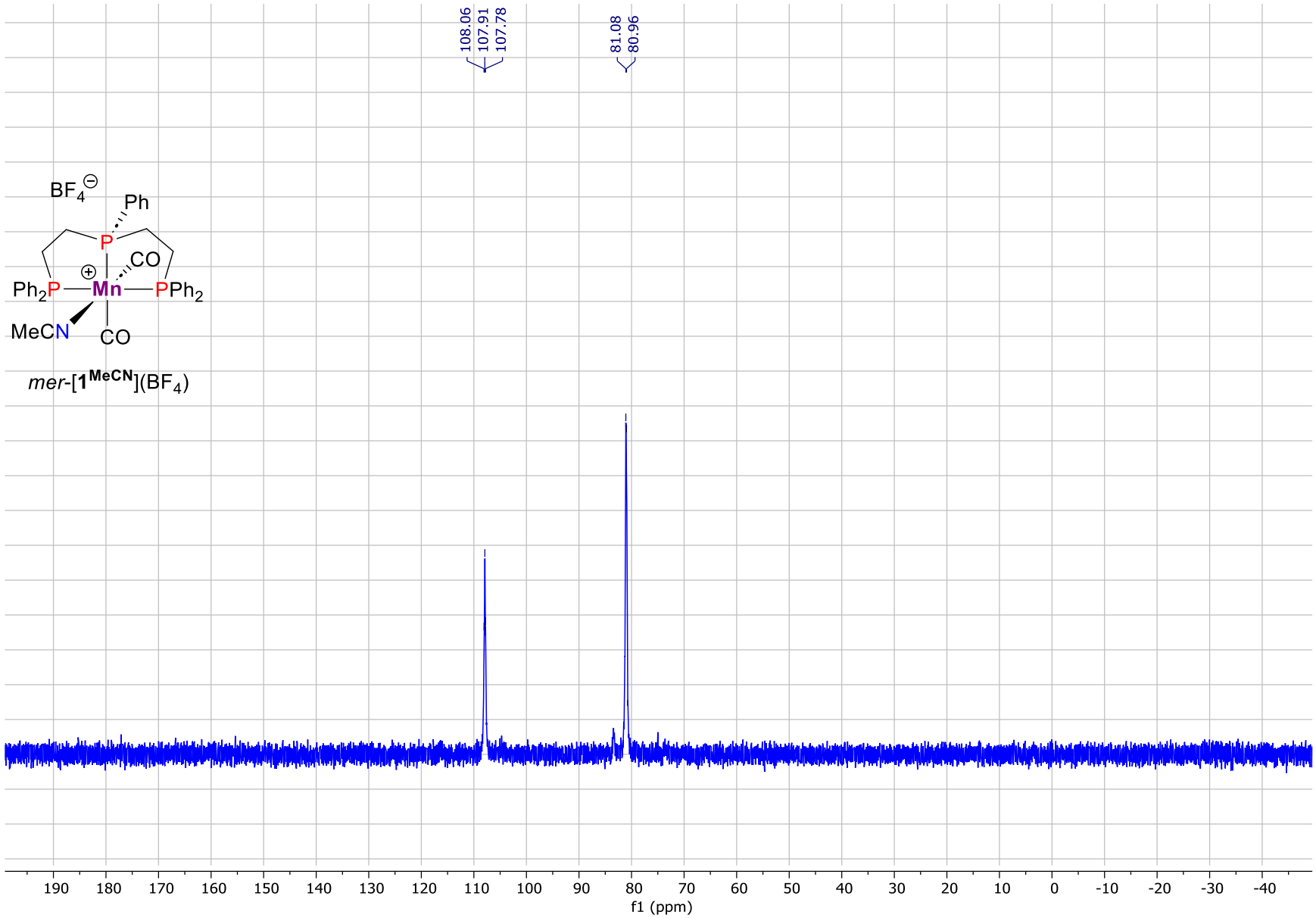

Figure S7. $^{31}P\{^{1}H\}$ NMR spectrum of complex *mer*-[**1**^{MeCN}](BF_4) (162.0 MHz, CD_2Cl_2, 298 K).

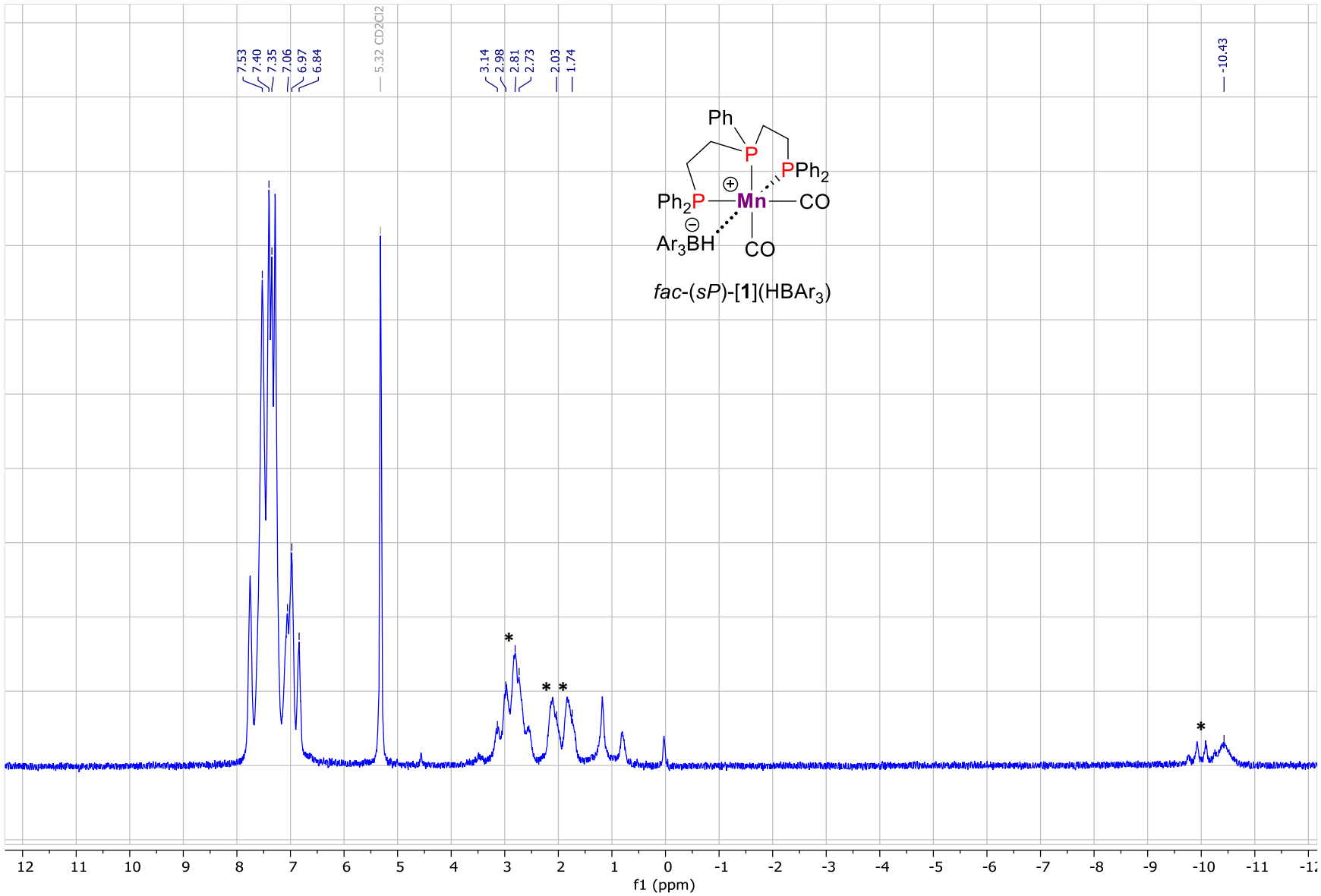

Figure S8. ^{1}H NMR spectrum of complex *fac-(sP)*-[**1**](BHAr$_3$) (300.1 MHz, CD_2Cl_2, 210 K), the signals of starting *mer*-**1**^{H} are marked with asterisk.

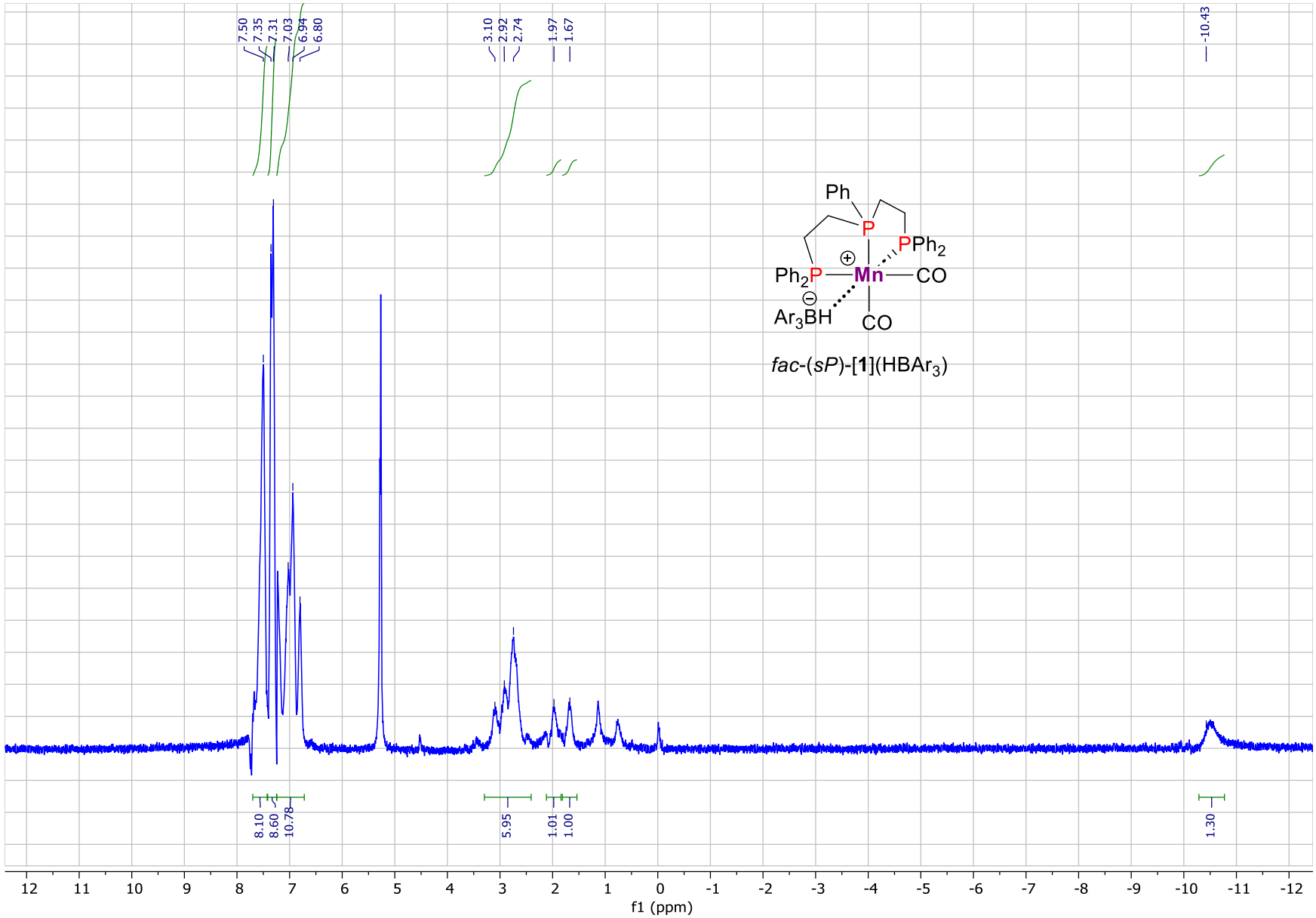

Figure S9. Mathematic subtraction of ^{1}H NMR spectrum of *mer*-**1**^{H} from spectrum of complex *fac-(sP)*-[**1**](BHAr$_3$) (300.1 MHz, CD_2Cl_2, 210 K).

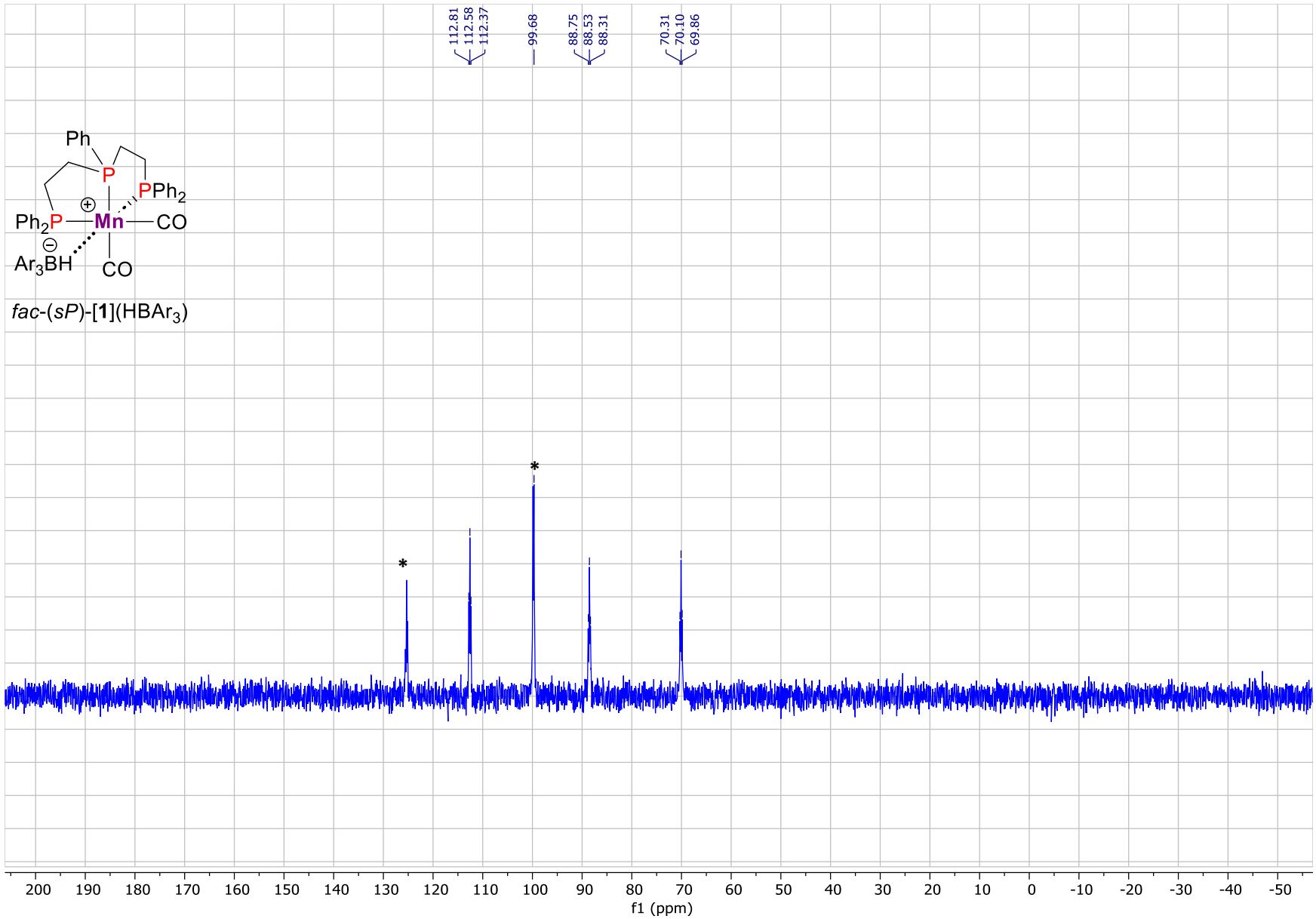

Figure S10. $^{31}P\{^{1}H\}$ NMR spectrum of complex *fac-(sP)*-[**1**](BHAr$_3$) (162.0 MHz, CD_2Cl_2, 210 K), the signals of starting *mer*-**1**^{H} are marked with asterisk.

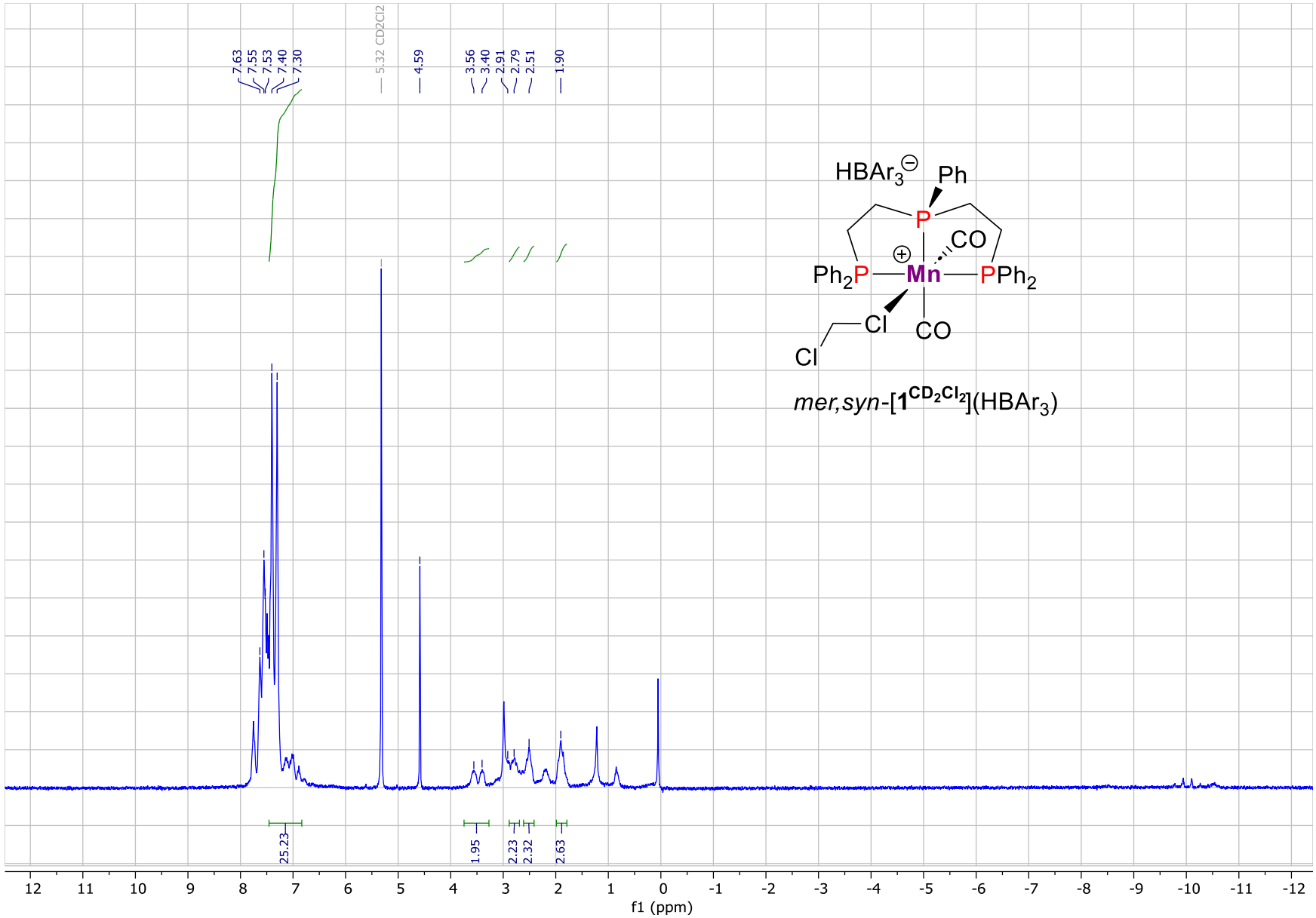

Figure S11. ^{1}H NMR spectrum of complex *mer,syn-(CO)*-[**1**^{CD_2Cl_2}](BHAr$_3$) (300.1 MHz, CD_2Cl_2, 250 K).

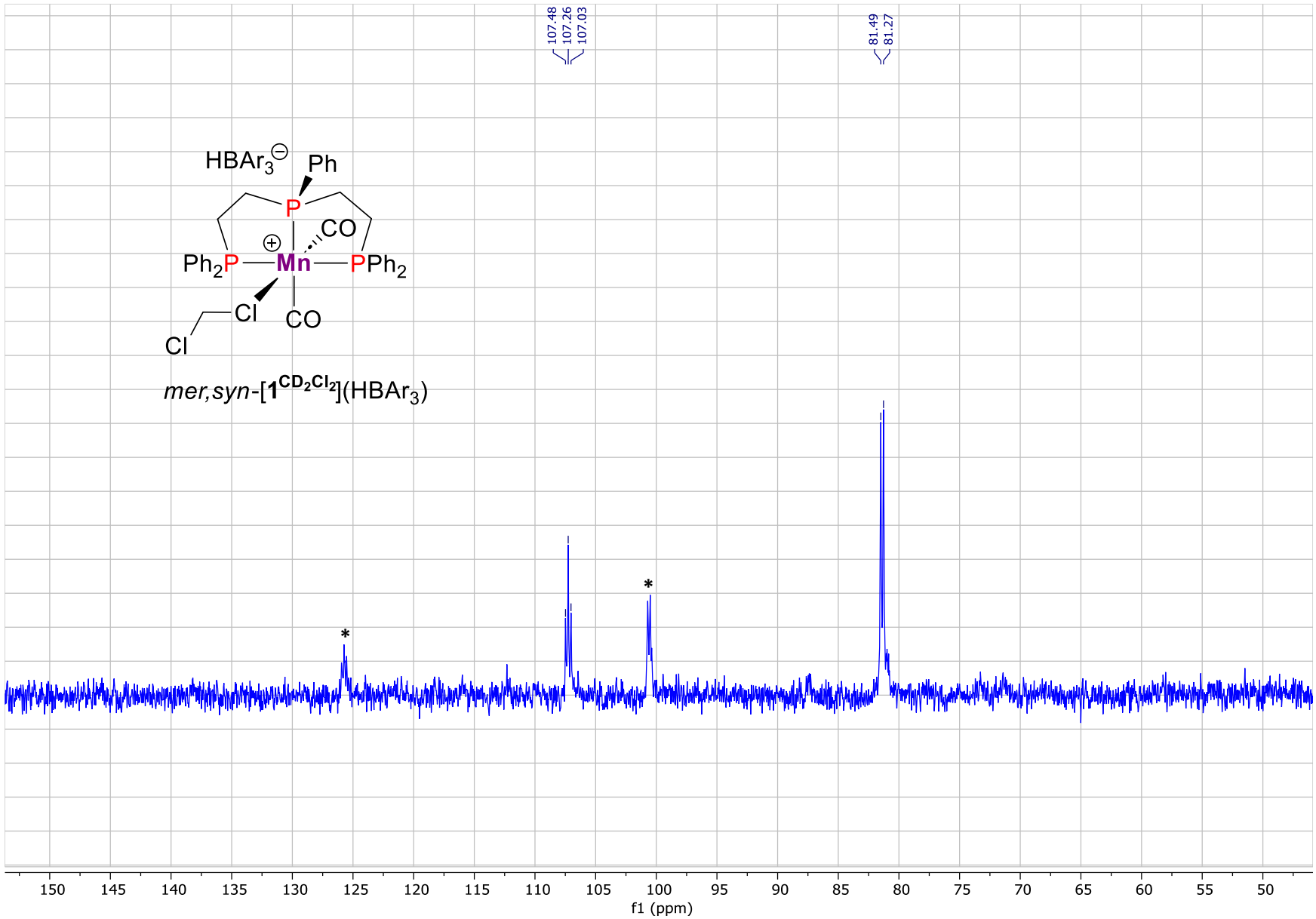

Figure S12. $^{31}P\{^{1}H\}$ NMR spectrum of complex *mer,syn-(CO)*-[**1**^{CD_2Cl_2}]($BHAr_3$) (162.0 MHz, CD_2Cl_2, 250 K), the signals of starting *mer*-**1**^{H} are marked with asterisk.

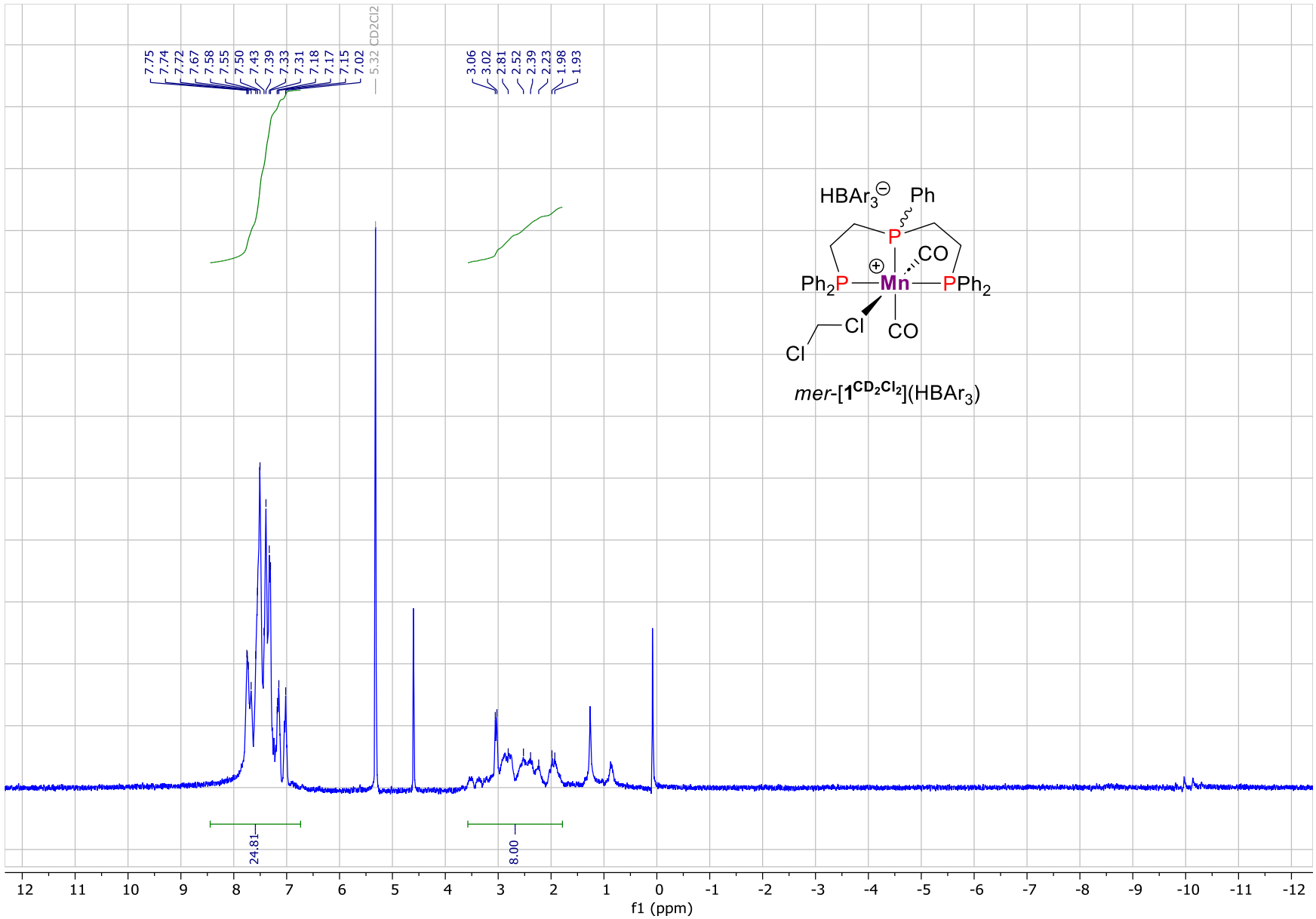

Figure S13. ^{1}H NMR spectrum of complex *mer-(CO)*-[**1**^{CD_2Cl_2}](BHAr$_3$) (300.1 MHz, CD_2Cl_2, 290 K).

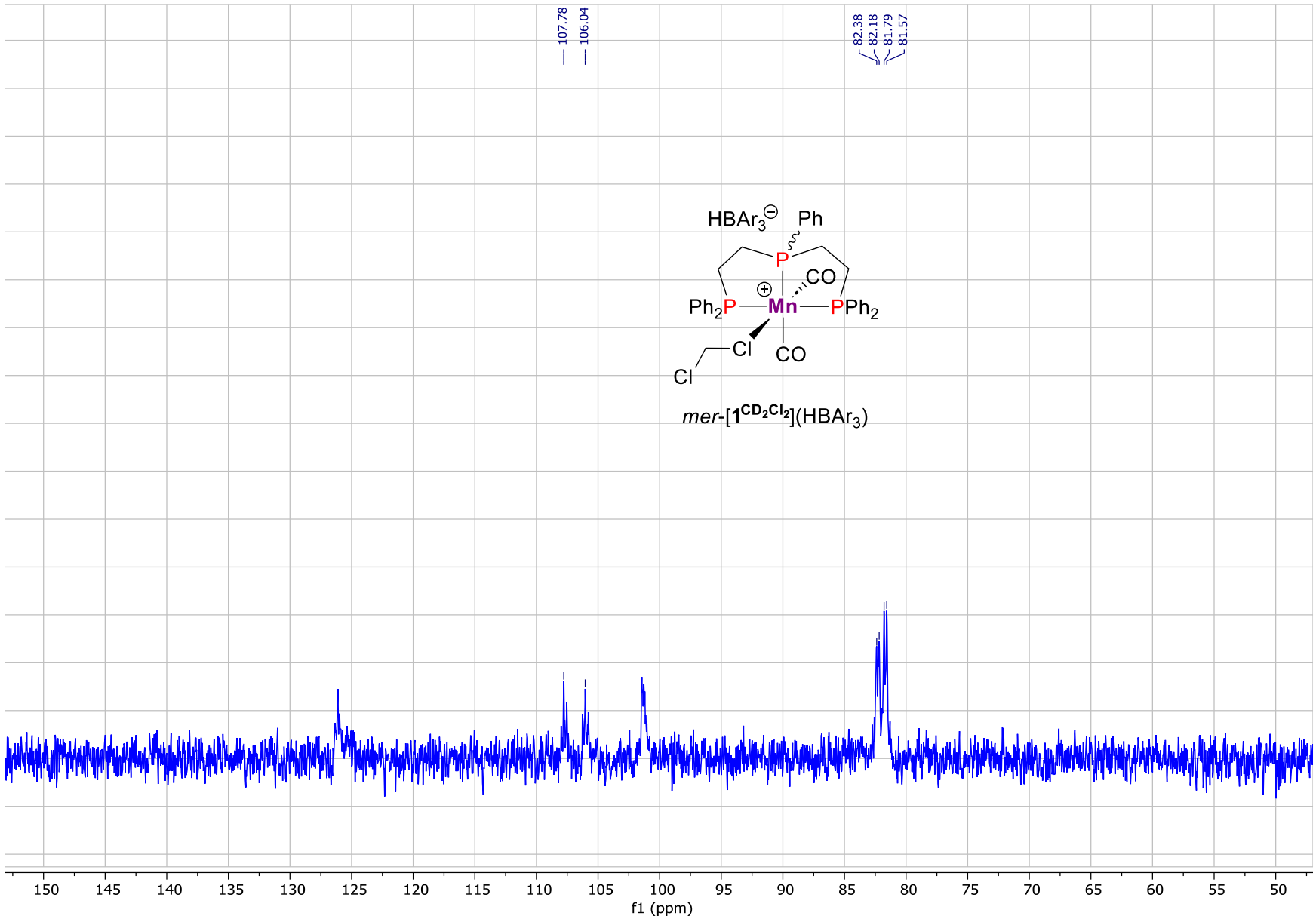

Figure S14. $^{31}P\{^{1}H\}$ NMR spectrum of complex *mer-(CO)*-[**1**^{CD_2Cl_2}](BHAr$_3$) (162.0 MHz, CD_2Cl_2, 290 K).

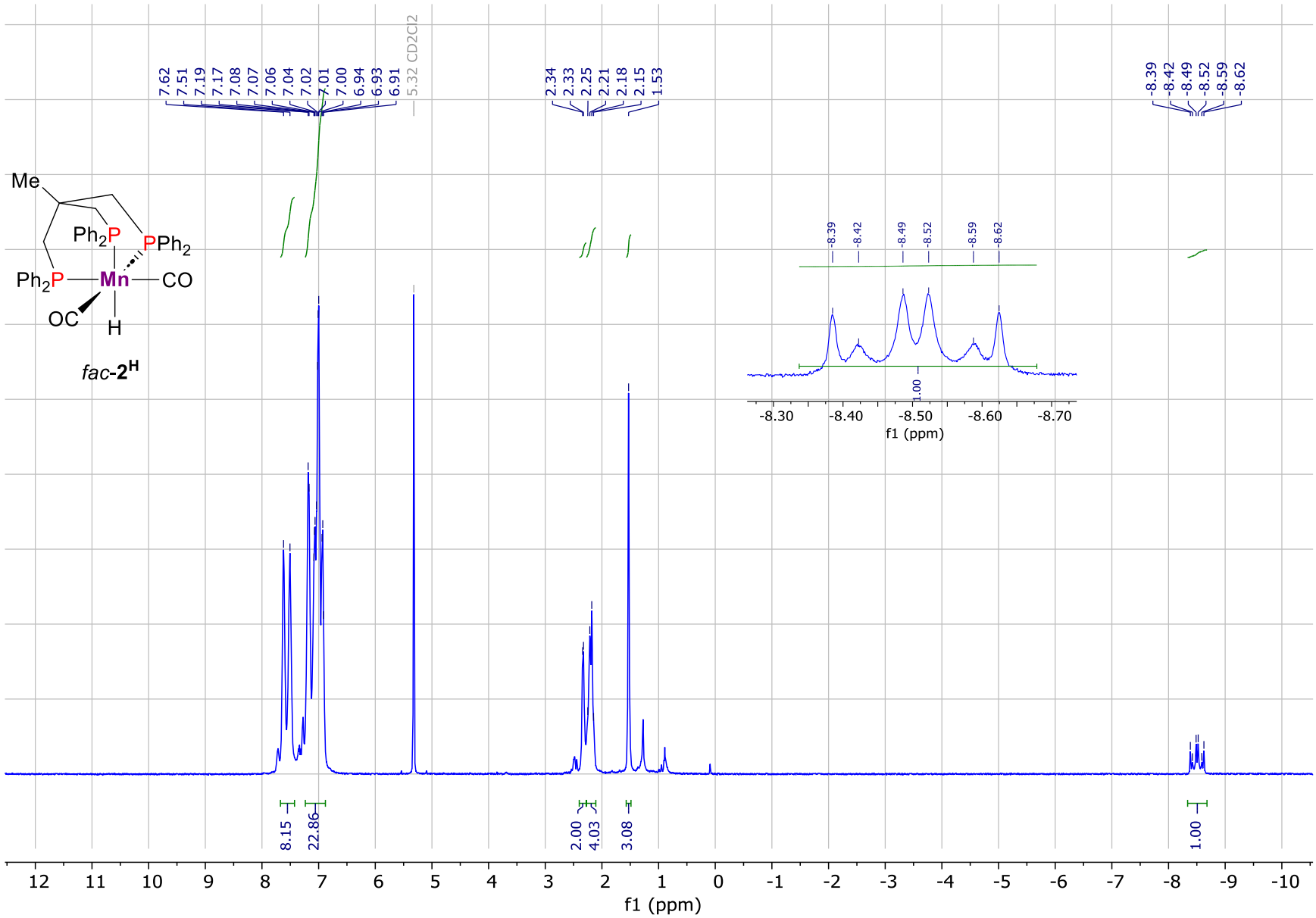

Figure S15. ^{1}H NMR spectrum of complex *fac*-**2^{H}** (400.1 MHz, CD_2Cl_2, 298 K).

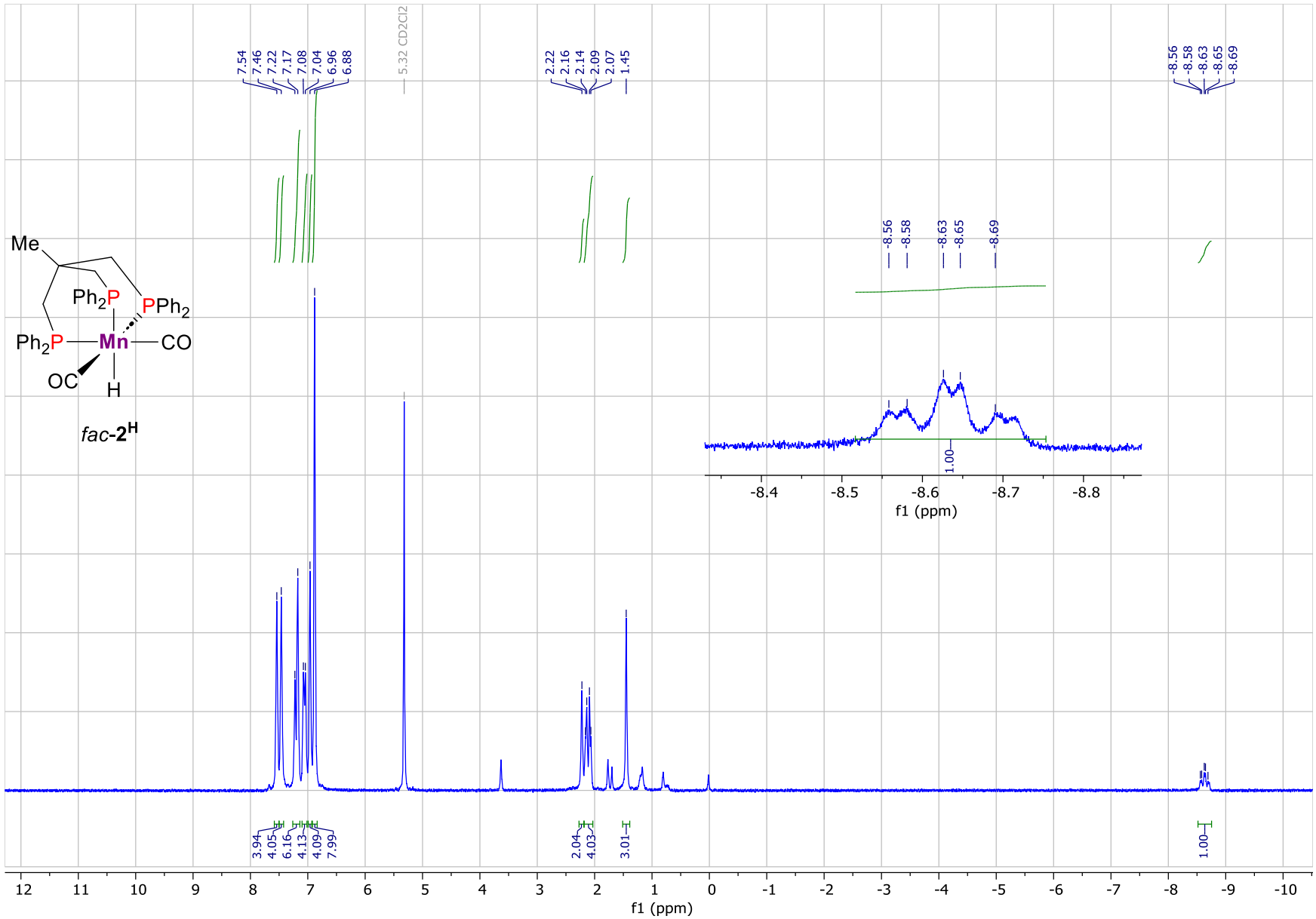

Figure S16. ^{1}H NMR spectrum of complex *fac*-**2^{H}** (600.1 MHz, CD_2Cl_2, 200 K).

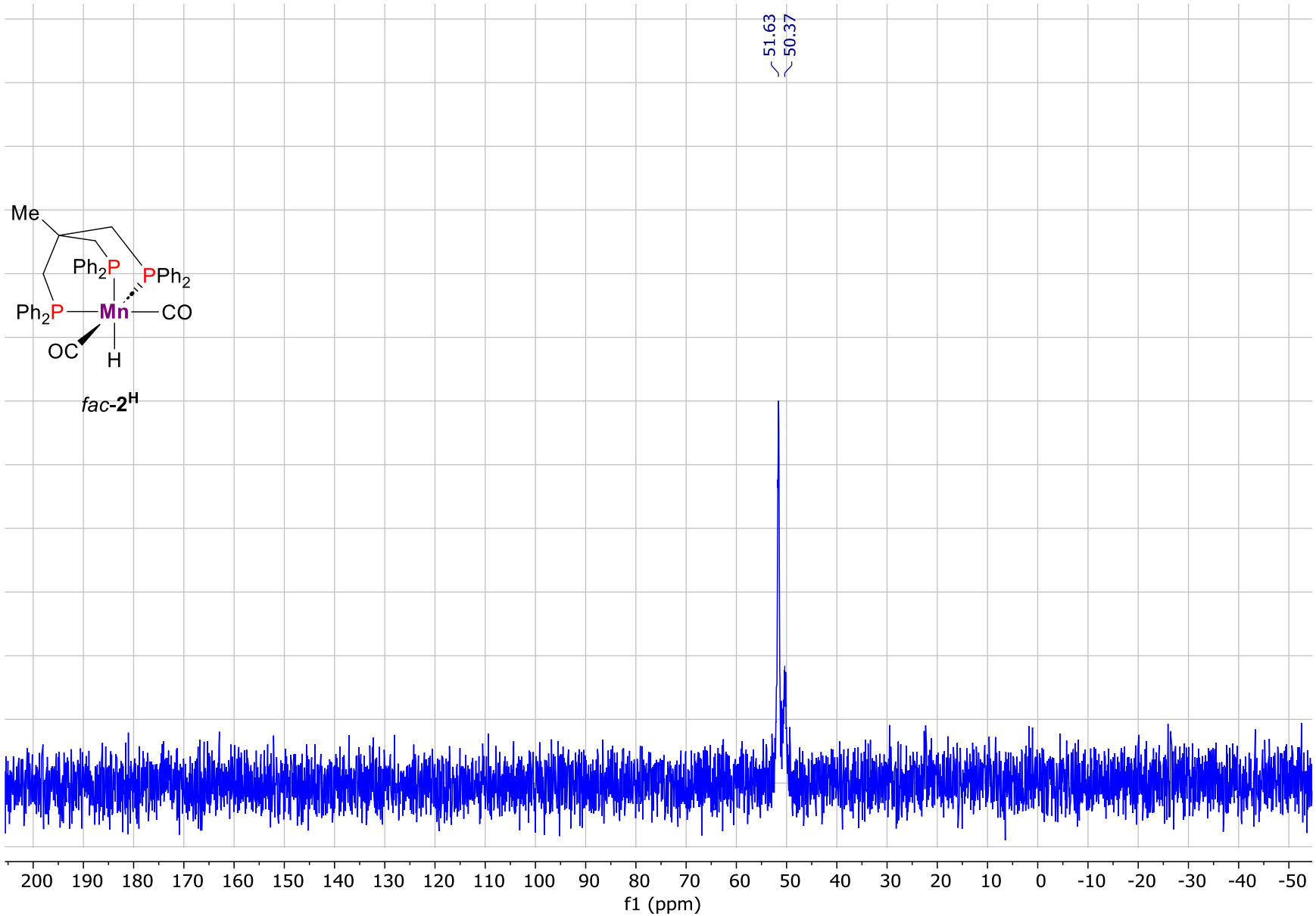

Figure S17. $^{31}P\{^{1}H\}$ NMR spectrum of complex *fac*-**2^{H}** (162.0 MHz, CD_2Cl_2, 298 K).

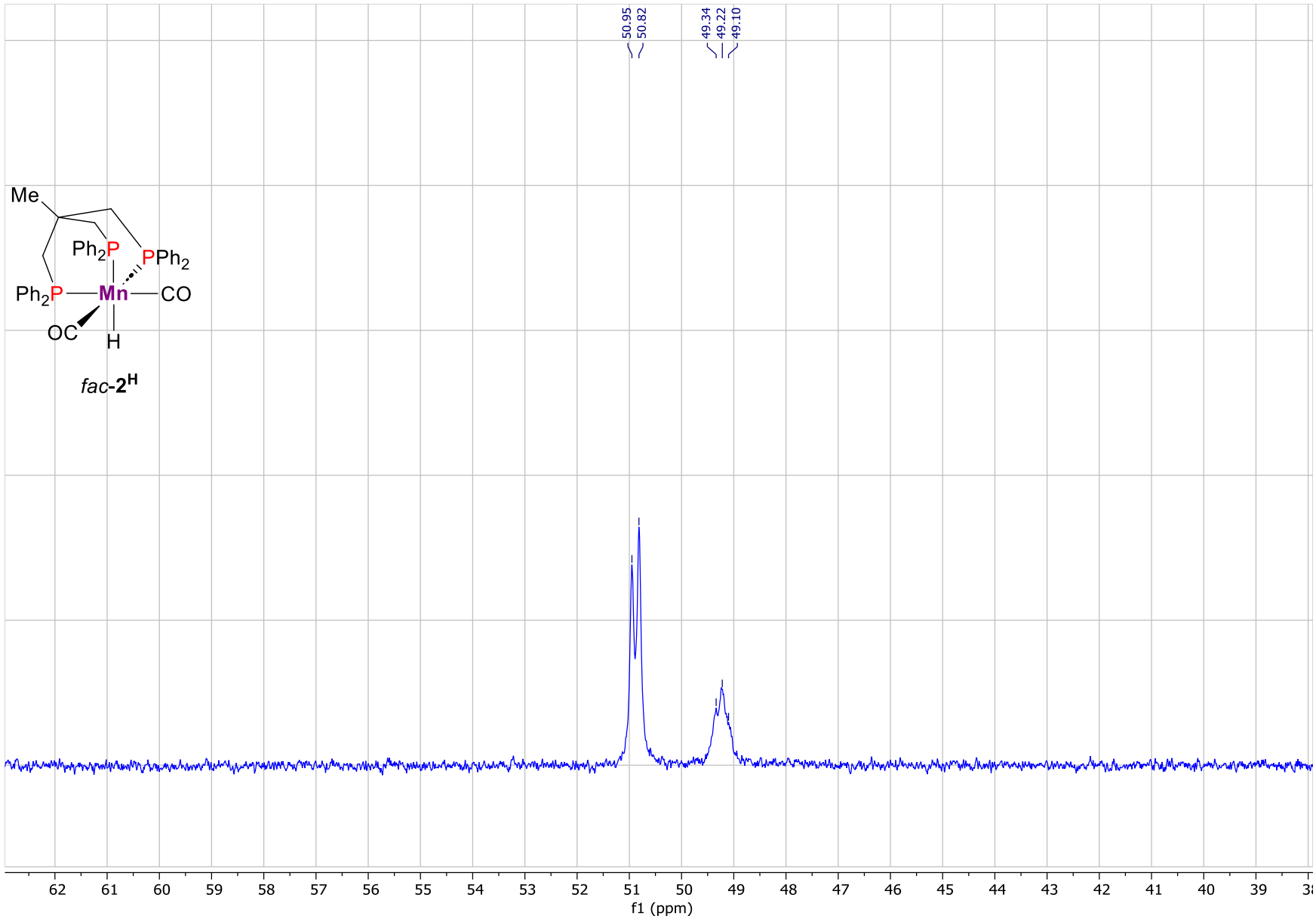

Figure S18. Section of $^{31}P\{^{1}H\}$ NMR spectrum of complex *fac*-**2**^{H} (243.0 MHz, CD_2Cl_2, 200 K).

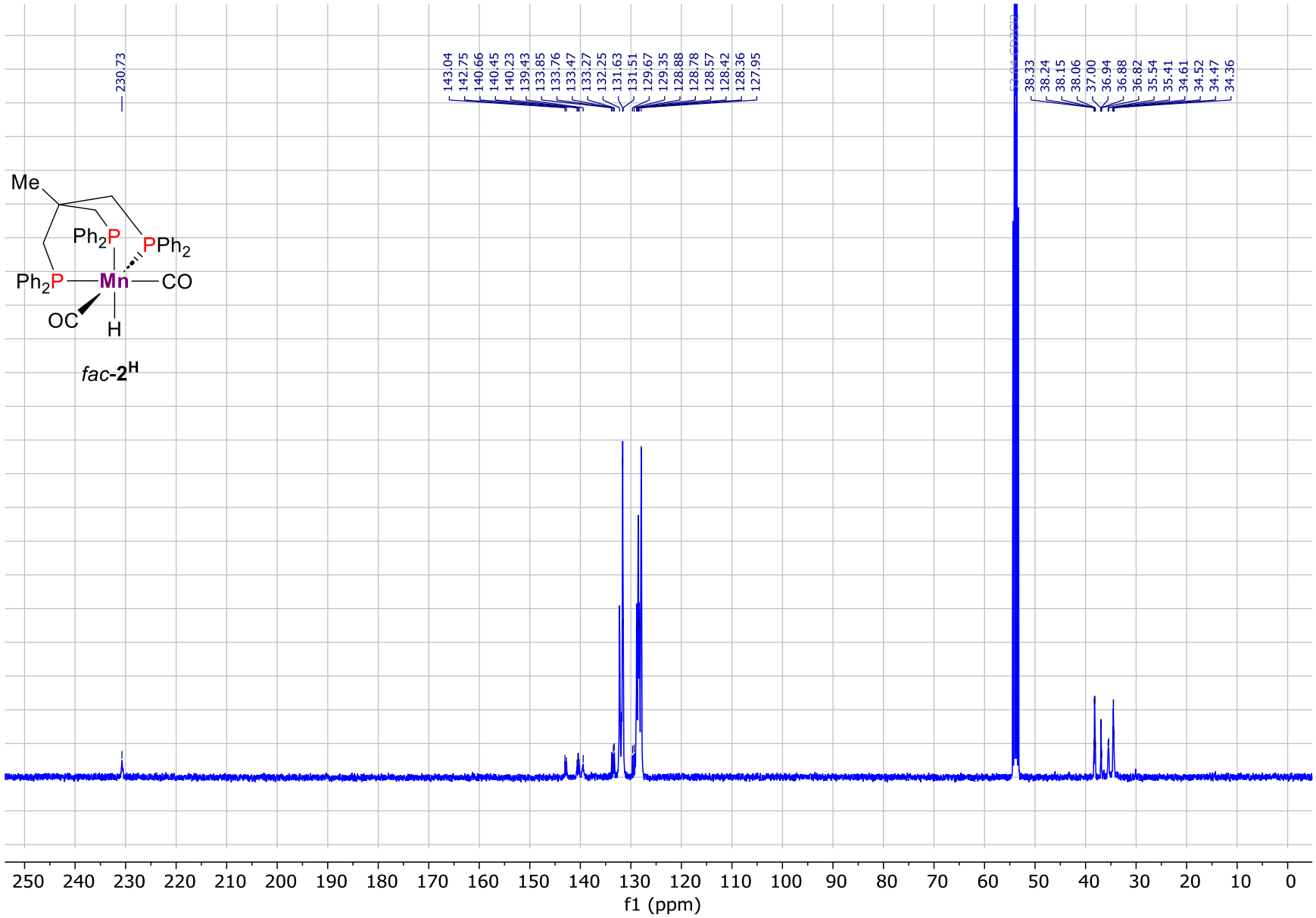

Figure S19. $^{13}C\{^{1}H\}$ NMR spectrum of complex *fac*-**2^{H}** (100.6 MHz, CD_2Cl_2, 298 K).

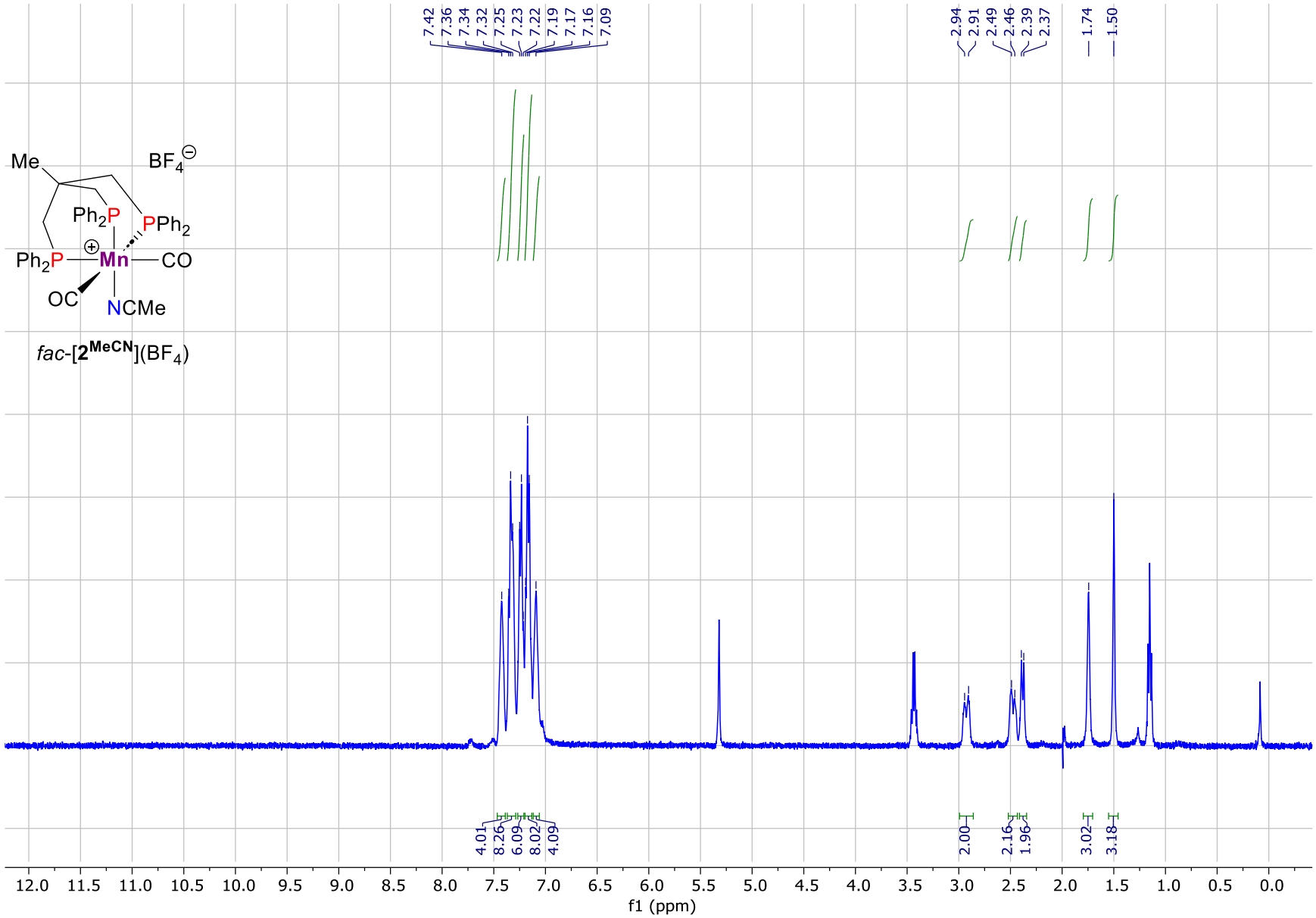

Figure S20. ^{1}H NMR spectrum of complex *fac*-[**2**$^{\mathbf{MeCN}}$](BF_4) (400.1 MHz, CD_2Cl_2, 298 K).

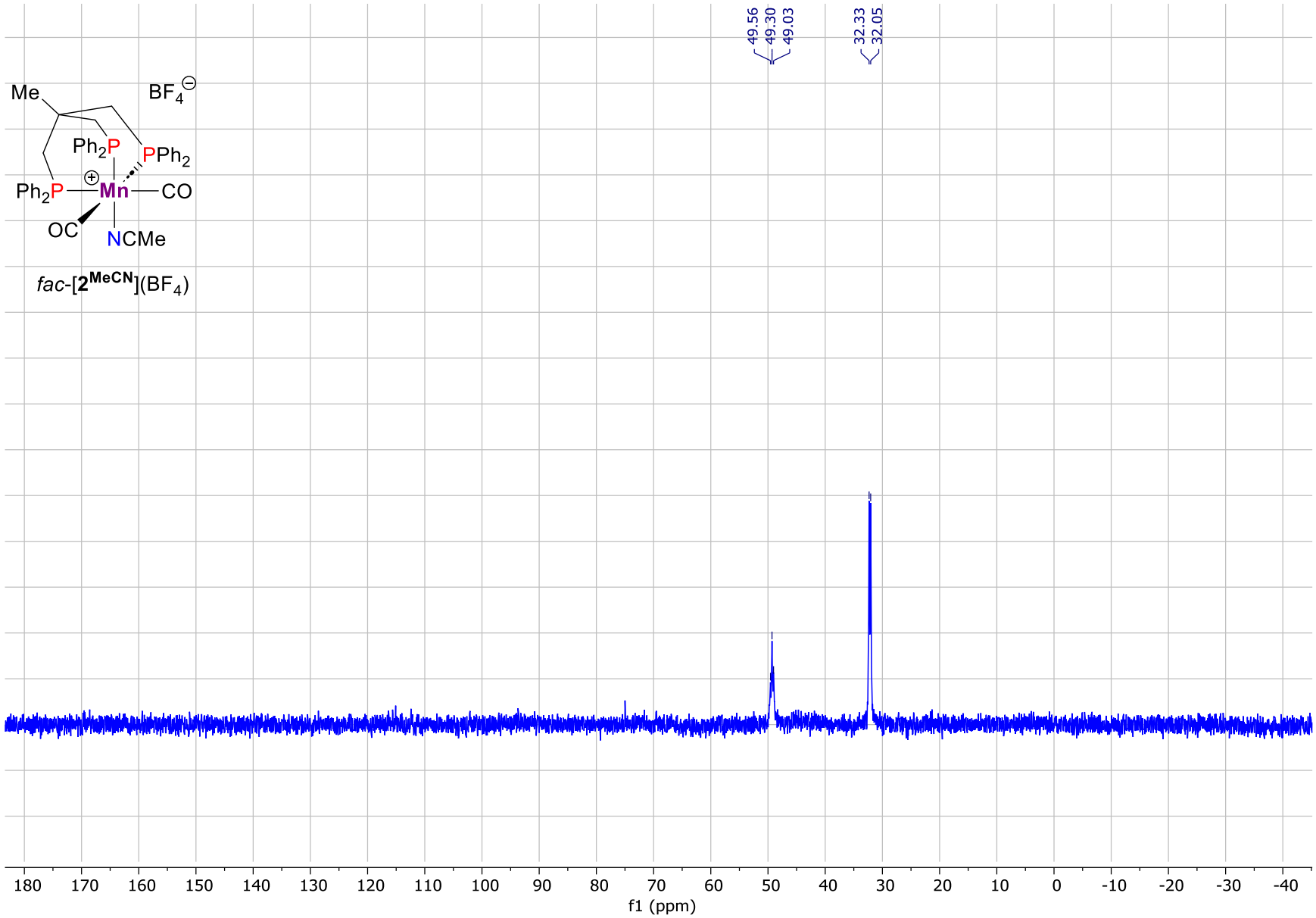

Figure S21. $^{31}P\{^{1}H\}$ NMR spectrum of complex *fac*-[**2**^{MeCN}](BF_4) (162.0 MHz, CD_2Cl_2, 298 K).

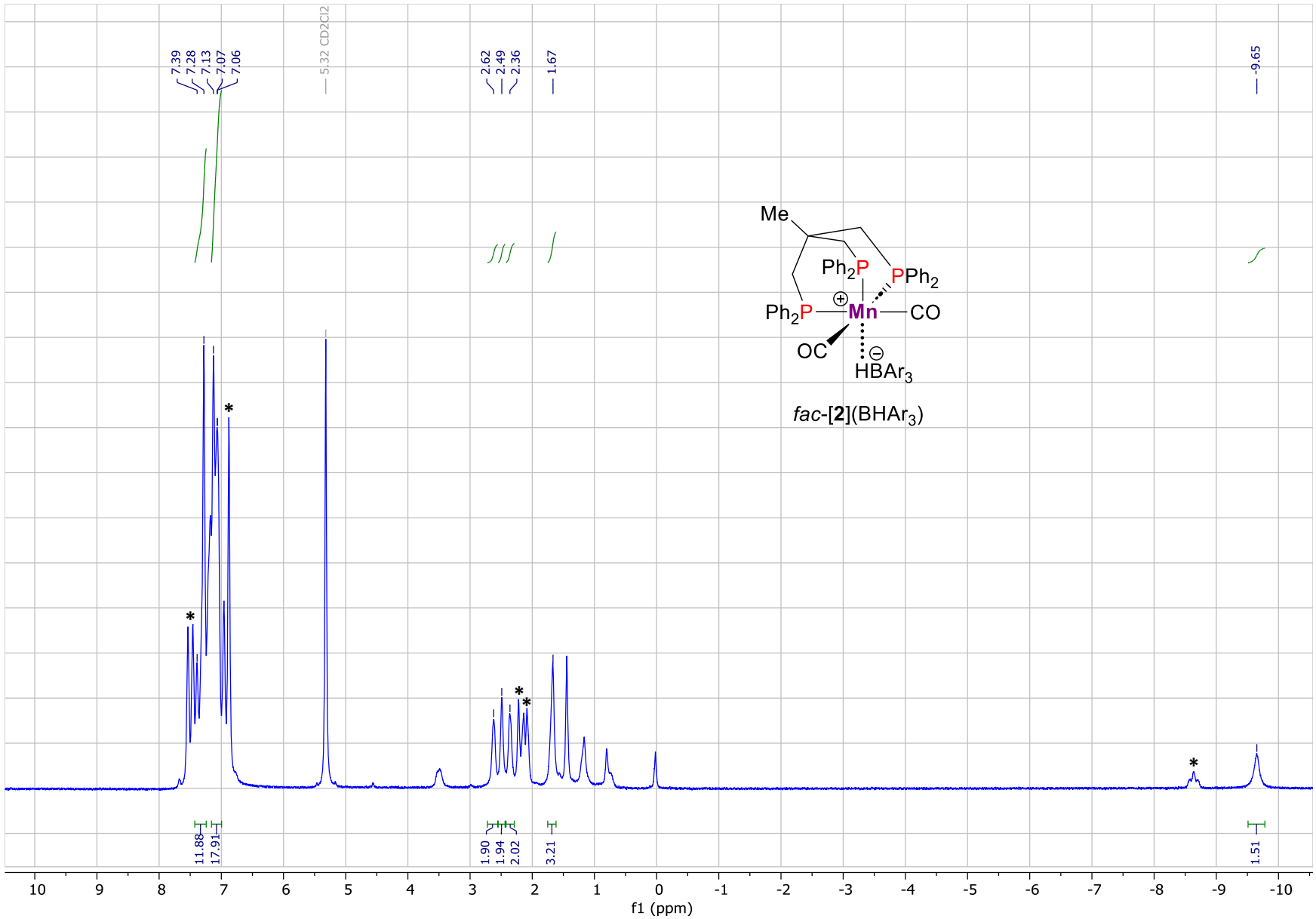

Figure S22. ^{1}H NMR spectrum of complex *fac*-[**2**](BHAr$_3$) (600.1 MHz, CD_2Cl_2, 200 K), the signals of starting *fac*-**2^{H}** are marked with asterisk.

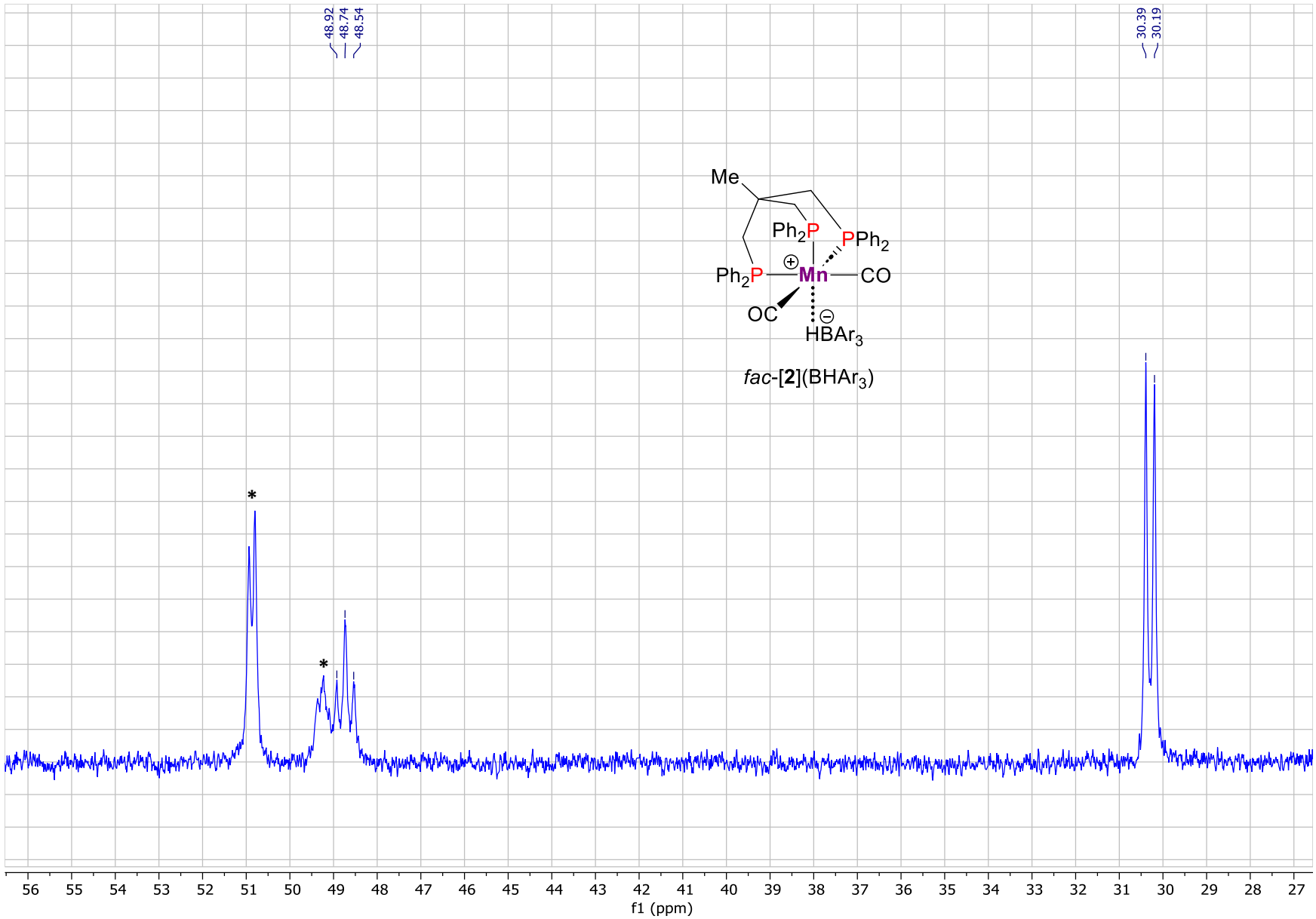

Figure S23. $^{31}P\{^{1}H\}$ NMR spectrum of complex *fac*-[**2**](BHAr$_3$) (243.0 MHz, CD_2Cl_2, 200 K), the signals of starting *fac*-**2**^{H} are marked with asterisk.

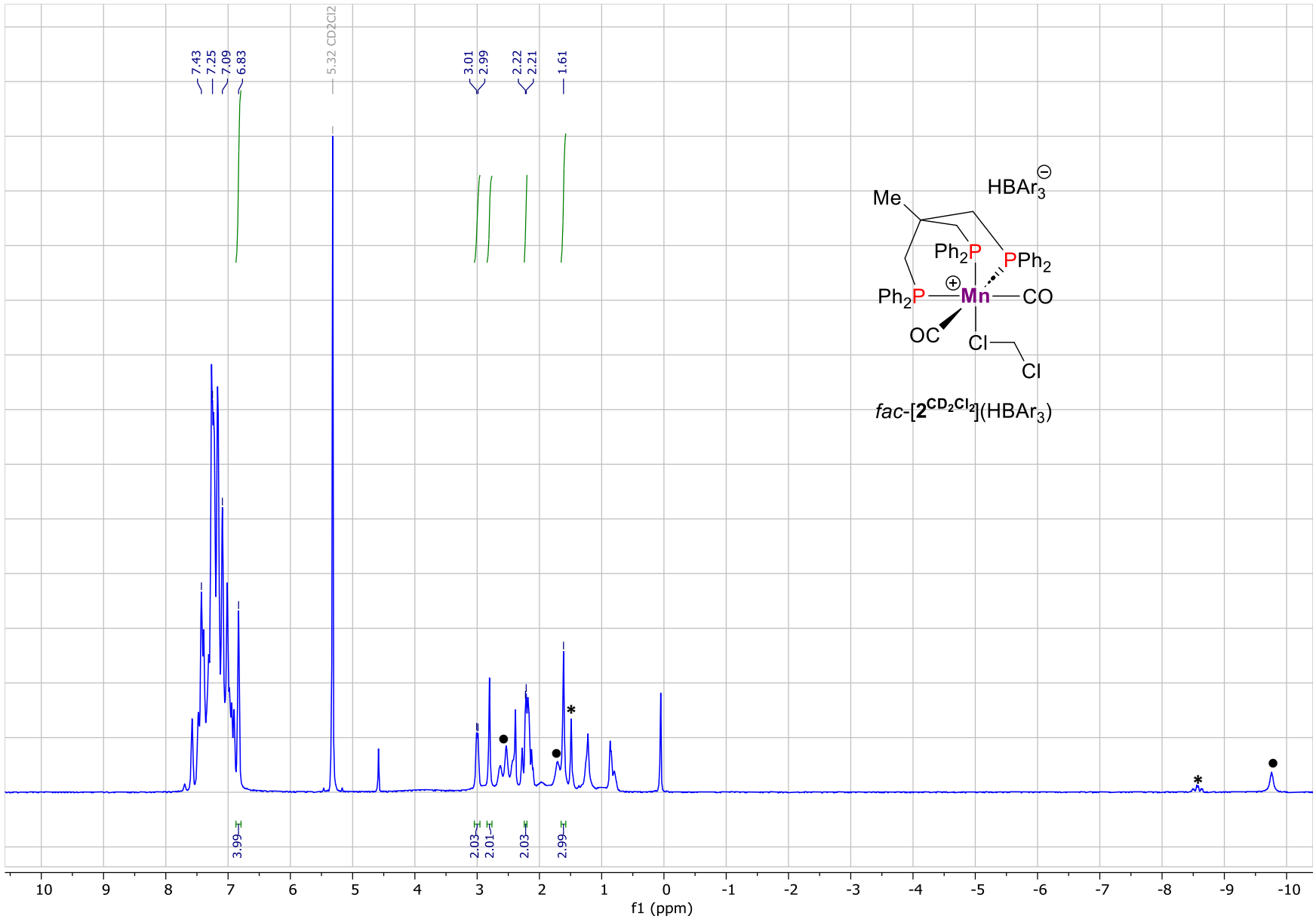

Figure S24. ^{1}H NMR spectrum of complex *fac*-[**2**^{CD_2Cl_2}](BHAr$_3$) (600.1 MHz, CD_2Cl_2, 250 K), the signals of *fac*-**2**^{H} and *fac*-[**2**](BHAr$_3$) are marked with * and ●, respectively.

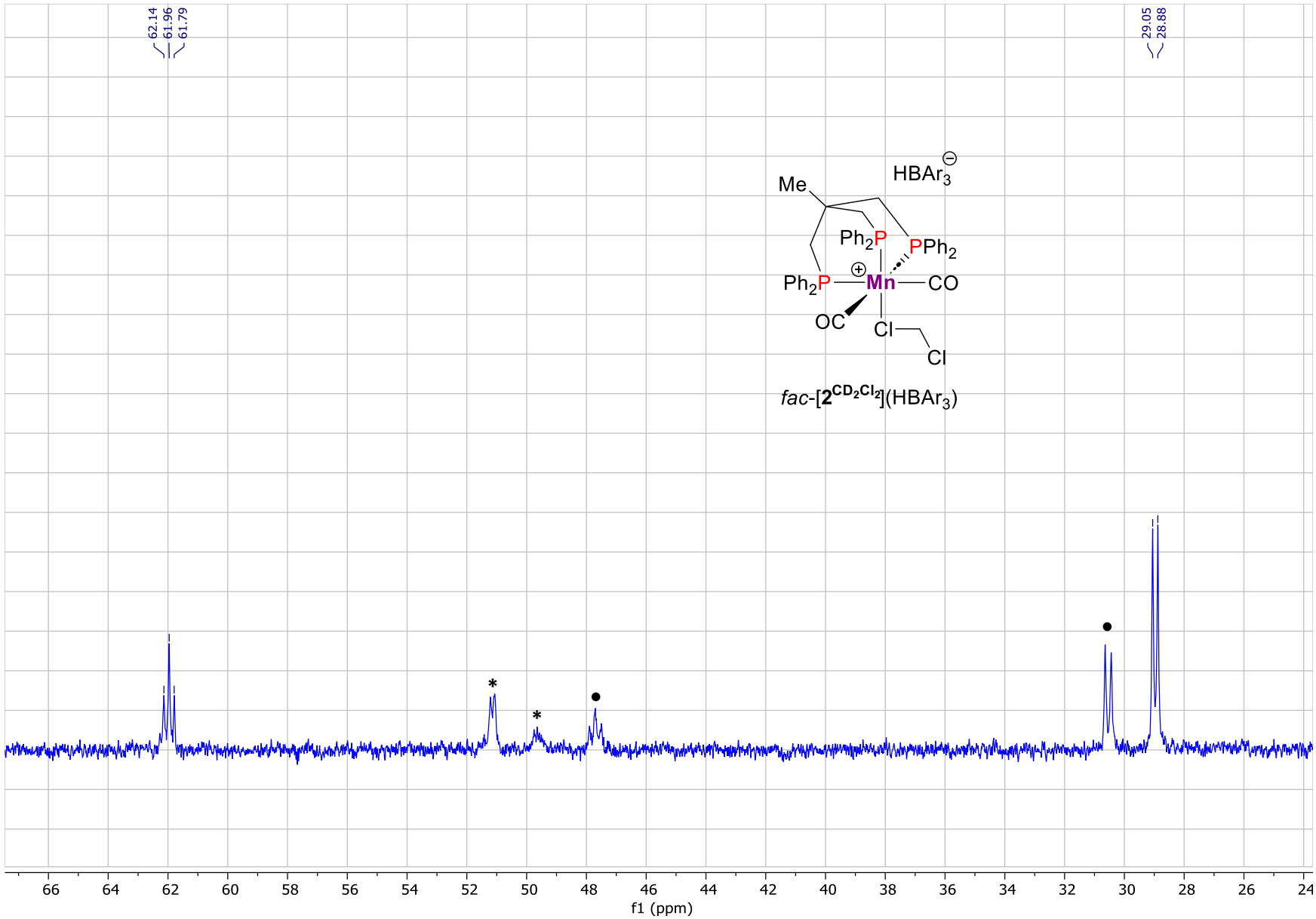

Figure S25. $^{31}P\{^{1}H\}$ NMR spectrum of complex *fac*-[**2**^{CD_2Cl_2}](BHAr$_3$) (243.0 MHz, CD_2Cl_2, 250 K), the signals of *fac*-**2**^{H} and *fac*-[**2**](BHAr$_3$) are marked with * and ●, respectively.

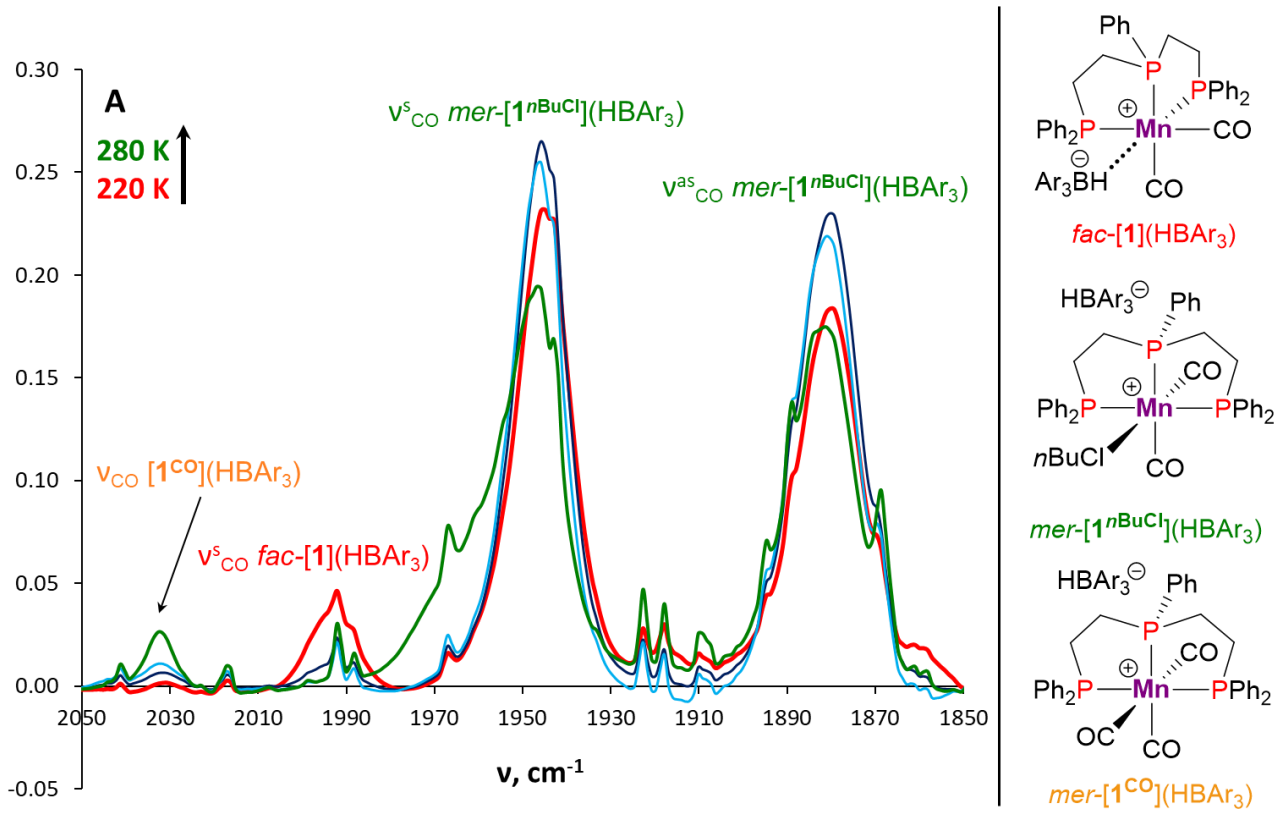

Figure S26. Variable temperature IR spectra of the *mer*-**1**^{H} and 1.5 equiv. $B(C_6F_5)_3$ mixture in 220-280 K range after keeping at 220 K for one hour (see Figure 2 in the main text). Experimental conditions: *n*BuCl, *c* = 0.003 M, *l* = 0.05 cm.

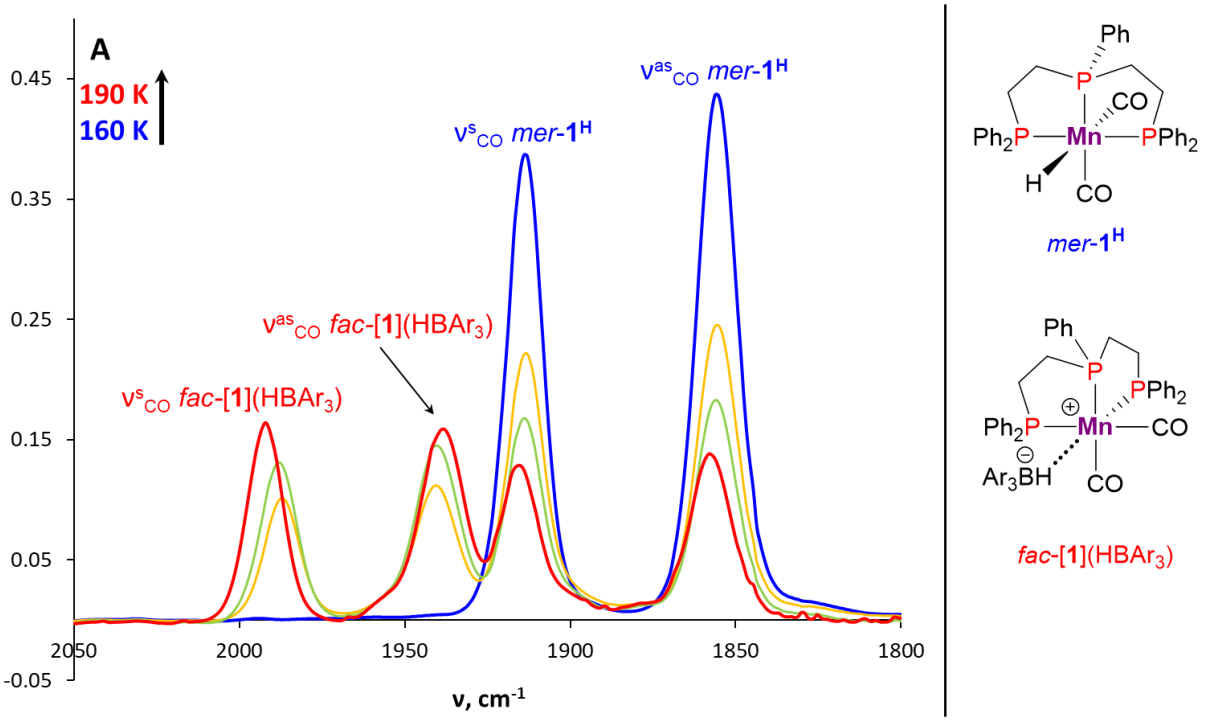

Figure S27. IR spectra of *mer*-**1**^{H} (blue line) and its mixture with 1.5 equiv. of $B(C_6F_5)_3$ at 160 K (orange line), 170 K (green line), 190 K (red line). *n*BuCl, c = 0.003 M, l = 0.05 cm.1

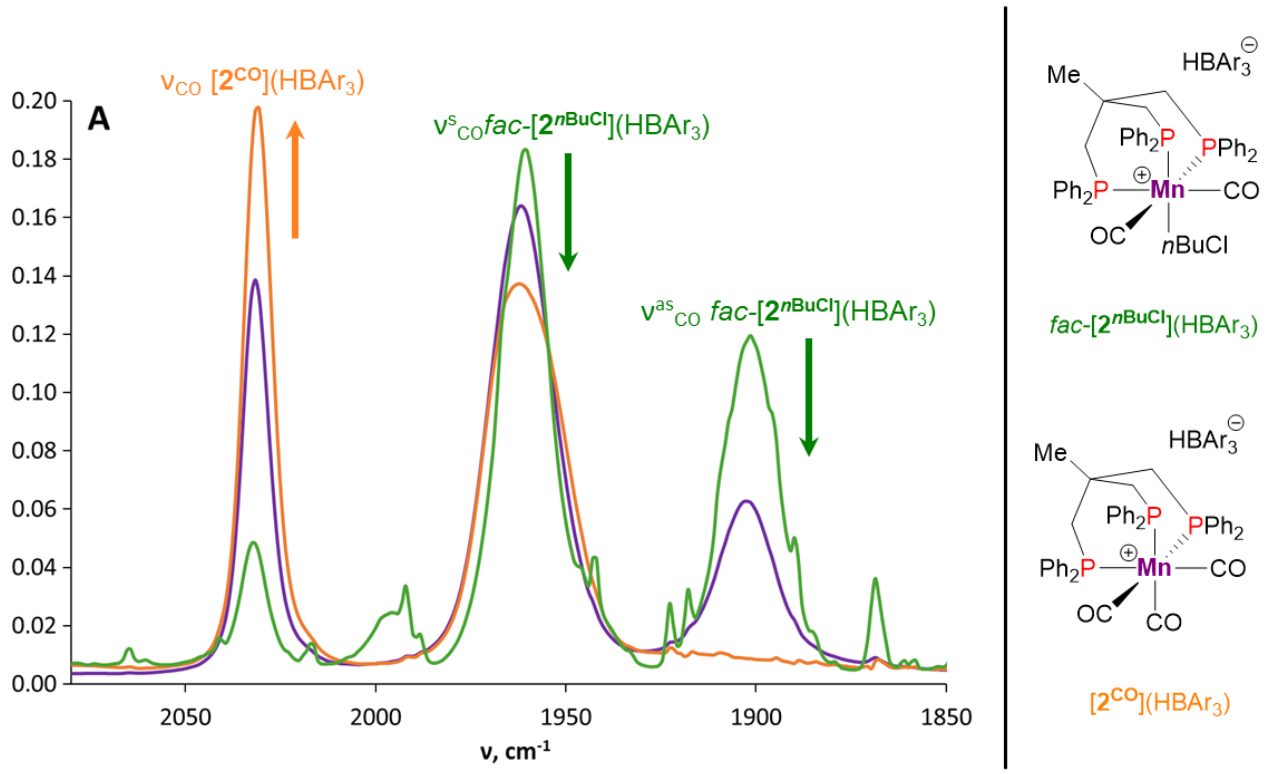

Figure S28. IR spectra of equimolar mixture *fac*-**2**^{H} and $B(C_6F_5)_3$ at 260 K (green line), at 298 K (purple line) and after CO bubbling (orange line). Experimental conditions: *n*BuCl, *c* = 0.0016 M, *l* = 0.1 cm.

Kinetic study of the hydrogen abstraction from complexes *mer*-**1**^{H} and *fac*-**2**^{H} to Lewis acid

For the hydride abstraction reaction from the complexes **1**^{H} and **2**^{H} to $B(C_6F_5)_3$ current concentrations of the components were calculated from the absorptions using Beer's law ($A = \varepsilon \cdot l \cdot c$) obtained by IR monitoring (decrease of ν_{CO} for the initial hydride) at the temperature range (160 – 230 K) (Table S4). Molar extinction coefficients were obtained experimentally from the temperature dependence of absorptions of the ν_{CO} for the initial hydrides ($\varepsilon = l^{-1} \cdot c^{-1} \cdot (2.4 \cdot 10^{-3} \cdot T + 0.88)$). The effective rate constants (k_{eff}) were obtained by second-order law for reaction type A + B → C + D:

$a_0 = c_0(MnH) = c(MnH) + c(Mn^+)$
$b_0 = c_0(B(C_6F_5)_3) = c(B(C_6F_5)_3) + c(Mn^+)$
$a = c(MnH)$
$b = c(B(C_6F_5)_3)$

$$k = \frac{1}{t(a_o - b_0)} ln \frac{b_0(a_0 - a)}{a_0(b_0 - b)}$$

Table S4. Experimentally determined concentrations of the components for the reaction between *mer*-**1**^{H} and $B(C_6F_5)_3$ in *n*BuCl at 170 K.

Time, sec	A(*mer*-1^{H})	c(*mer*-1^{H})	c(*mer*-1^{+})	c(B(C$_6$F$_5$)$_3$)	1/(a$_0$-b$_0$)ln(b$_0$(a$_0$-a)/(a$_0$(b$_0$-b))
	0.437	**0.00281**	-	**0.00366**	-
0	0.256	0.00170	0.00110	0.00256	-
218	0.247	0.00164	0.00116	0.00250	13.986
443	0.239	0.00159	0.00122	0.00245	27.328
657	0.230	0.00153	0.00127	0.00239	41.883
804	0.223	0.00148	0.00132	0.00234	56.266
992	0.216	0.00144	0.00137	0.00229	69.756
1159	0.211	0.00140	0.00140	0.00226	80.184
1325	0.203	0.00135	0.00145	0.00221	96.976

ε(170 K) = 3002.156 l·mol^{-1}·cm^{-1}

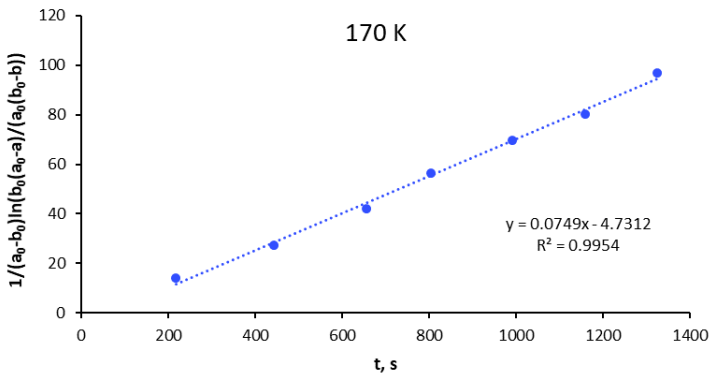

Figure S29. Plot for the determination of the effective rate constant (k_{eff}) in the reaction between *mer*-**1**^{H} with $B(C_6F_5)_3$ in *n*BuCl at 170 K.

Then the corresponding activation parameters ($\Delta H^{\neq}$, $\Delta S^{\neq}$, $\Delta G^{\neq}_{298K}$) were determined with Eyring's equation for bimolecular reaction in solution at 160 – 230 K temperature range (Figure S30-S31):

$$-ln\left(\frac{k_{eff} \cdot h}{T \cdot k_B}\right) = \frac{\Delta H^{\neq}}{RT} - \frac{\Delta S^{\neq}}{R}$$

Table S5. Calculated effective rate constants (k_{eff}) from the experimental data obtained for the reaction of *mer*-**1**^{H} with $B(C_6F_5)_3$ at 170-200 K.

T, K	1/T	k_{eff}	$-\ln(k_{eff}*h*(1/T)/k_B)$
170	0.005882	**0.0749**	31.4863
180	0.005556	**0.1107**	31.1528
190	0.005263	**0.2050**	30.5907
200	0.005000	**0.4785**	29.7943

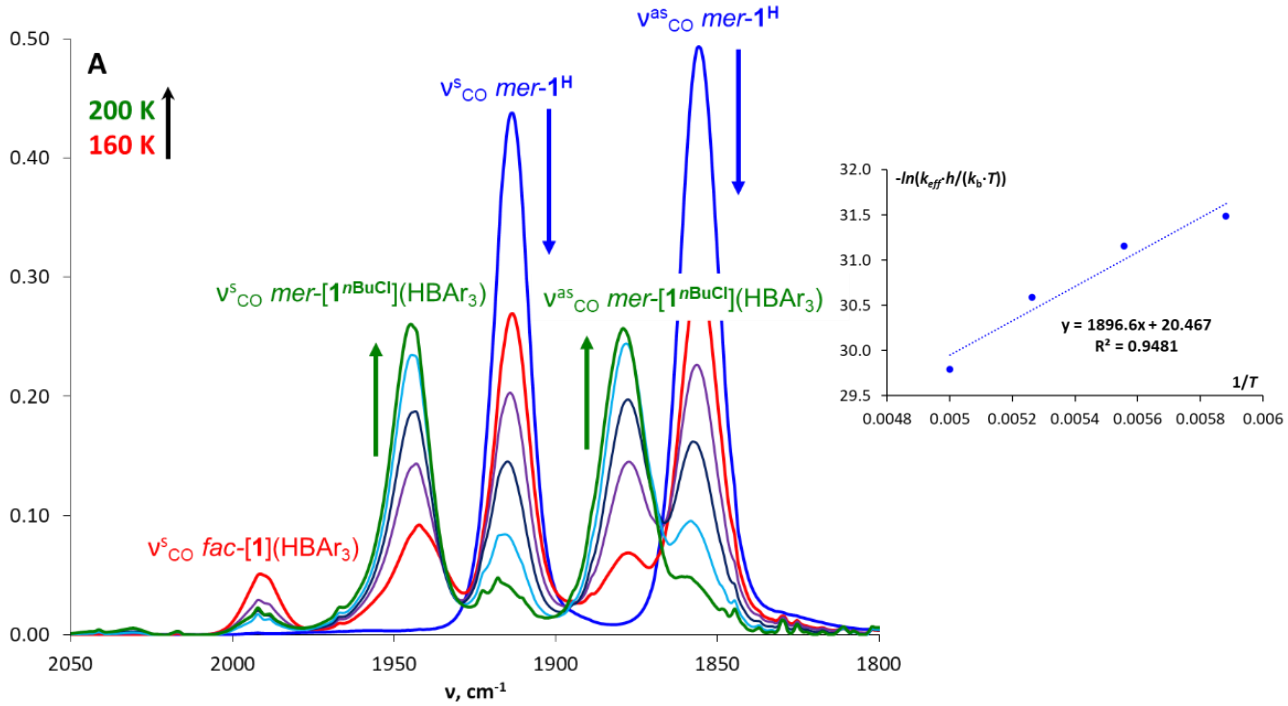

Figure S30. IR monitoring of the reaction of complex *mer*-**1**^{H} (blue line) with 1.3 equiv. of $B(C_6F_5)_3$ starting from 160 K (red line) and ending at 200 K (green line) and the Eyring plot of effective rate constants vs reversed temperature (at the right). Experimental conditions: *n*BuCl, *c* = 0.0028 M, *l* = 0.05 cm.

Table S6. Calculated effective rate constants (k_{eff}) from the experimental data obtained for the reaction of *fac*-**2**^{H} with $B(C_6F_5)_3$ at 190−230 K.

T, K	1/T	k_{eff}	$-\ln(k_{eff}*h*(1/T)/k_B)$
190	0.005263	**0.0443**	32.1223
210	0.004762	**0.2014**	30.7085
220	0.004545	**1.4582**	28.7753
230	0.004348	**2.8100**	28.1638

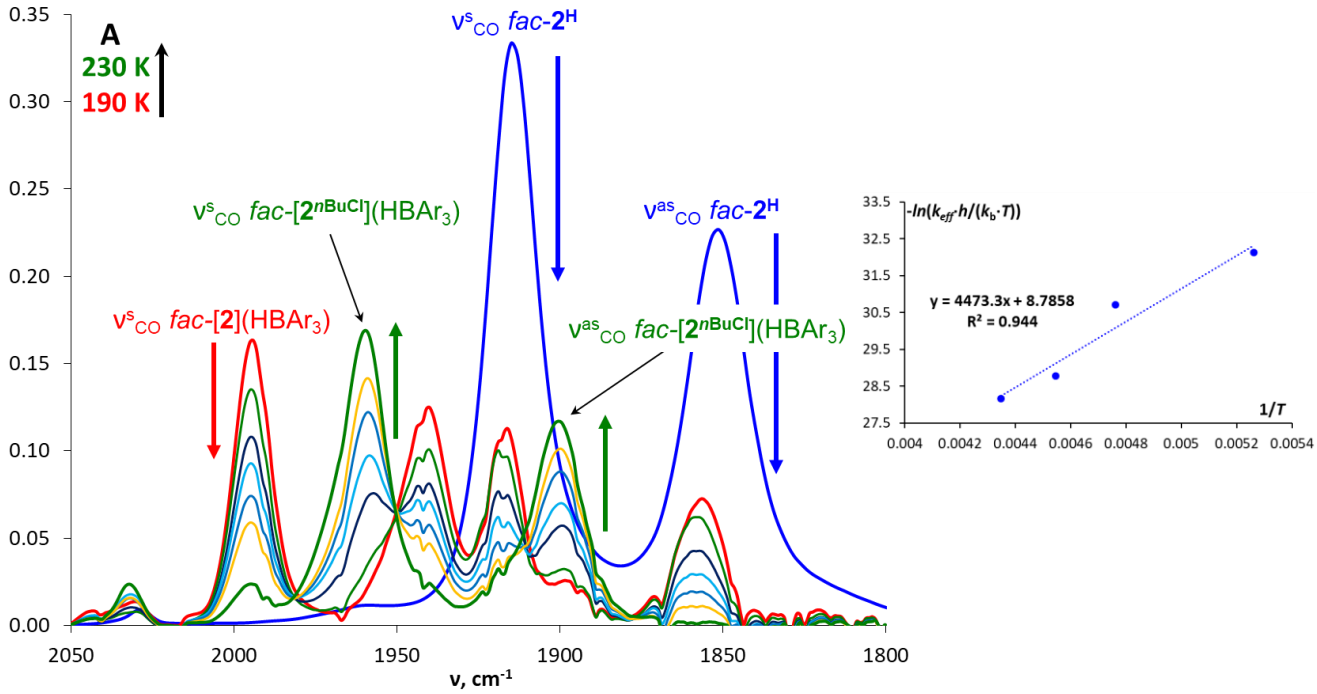

Figure S31. IR monitoring of the reaction of complex *fac*-**2**^{H} (blue line) with 1.5 equiv. of $B(C_6F_5)_3$ starting from 190 K (red line) and ending at 230 K (green line) and the Eyring plot of effective rate constants vs reversed temperature (at the right). Experimental conditions: *n*BuCl, *c* = 0.0016 M, *l* = 0.1 cm.

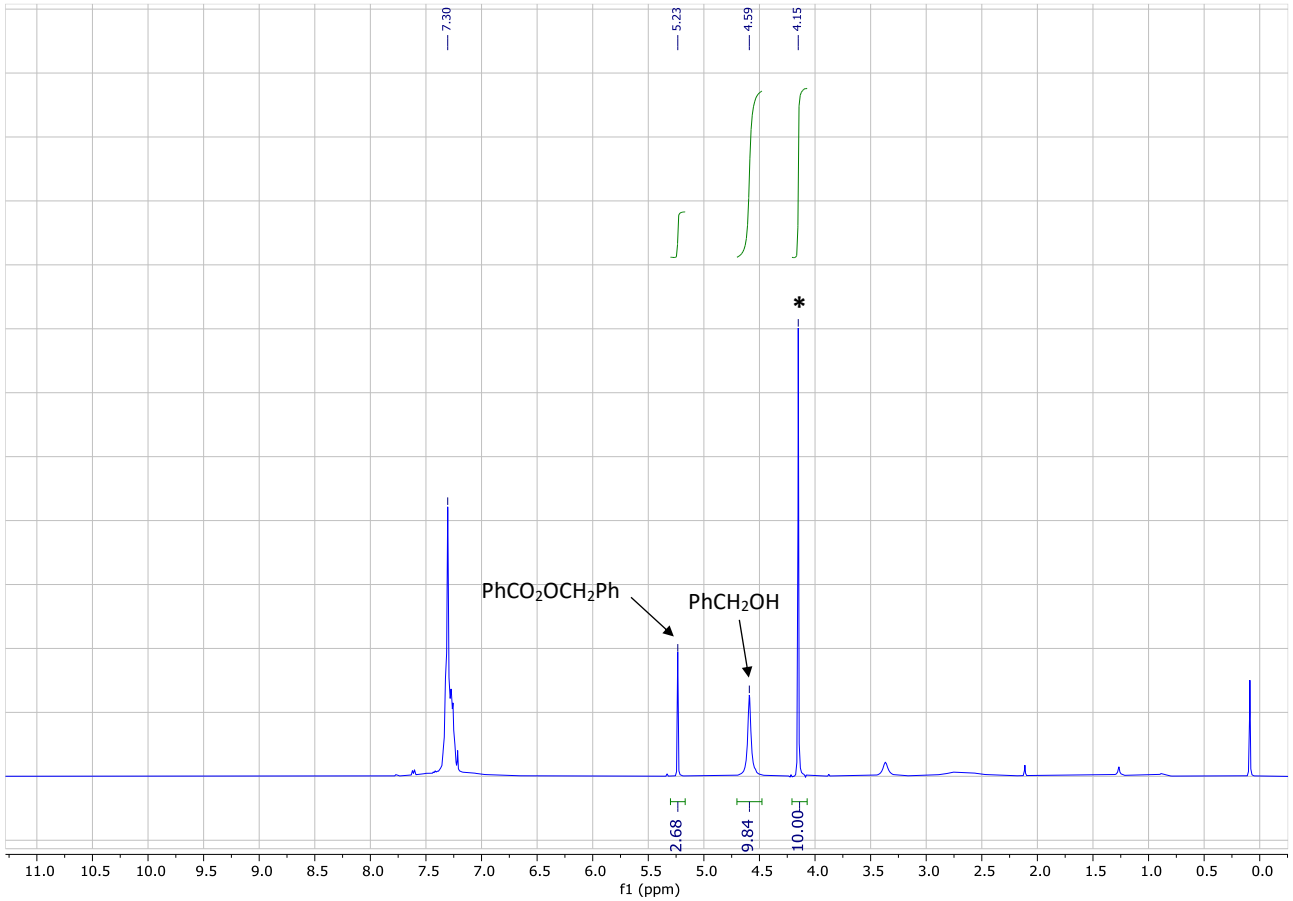

Figure S32. ^{1}H NMR (400.1 MHz, $CDCl_3$) spectrum of crude product obtained from the hydrosilylation of benzyl benzoate catalyzed by complex *mer*-**1**^{Br} (the signal of ferrocene added as internal standard is indicated with asterisk).

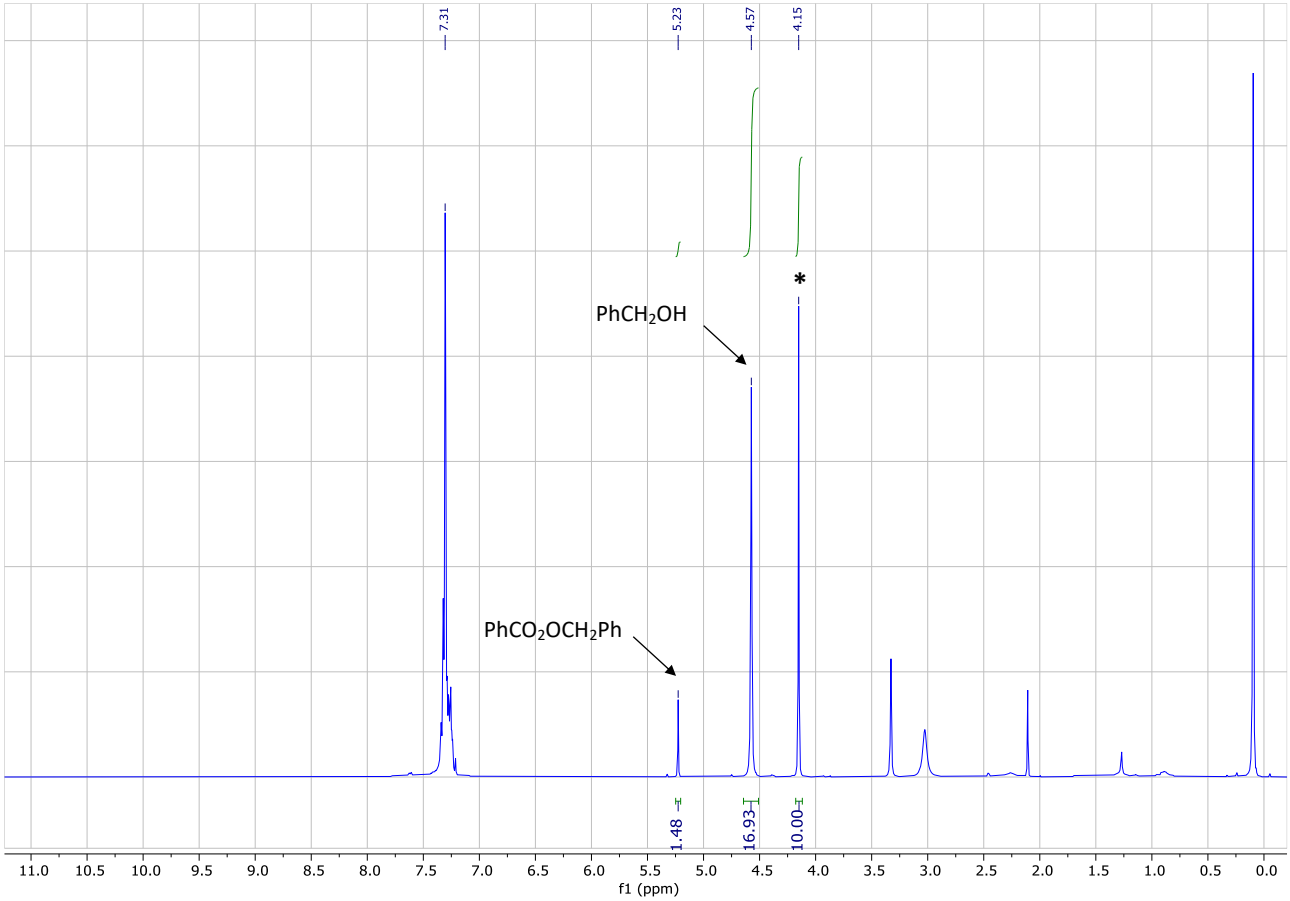

Figure S33. ^{1}H NMR (400.1 MHz, $CDCl_3$) spectrum of crude product obtained from the hydrosilylation of benzyl benzoate catalyzed by complex *fac*-**2**^{Br} (the signal of ferrocene added as internal standard is indicated with asterisk).

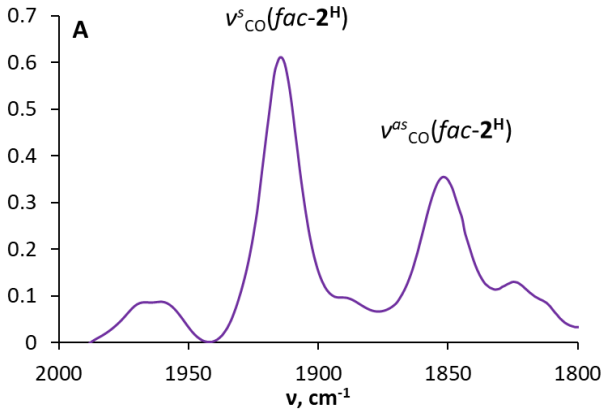

Figure S34. IR spectrum of the aliquot taken after 5 min of heating from the reaction mixture of *fac*-**2**^{Br}, benzyl benzoate and $PhSiH_3$. Experimental conditions: CH_2Cl_2, RT, *l* = 0.1 cm.